



**University of  
Reading**

**Department of Meteorology**

**MSc Dissertation**

**Response of convection to changes in the  
thermodynamic environment**

**Xiao Ma**

A dissertation submitted in partial fulfilment of the  
requirement for the degree of Master of Science in MSc  
Atmosphere, Ocean and Climate

**Supervisors:            Prof. Robert Stephen Plant  
                                  Dr. Chimene Daleu**

8 August 2018

## **Acknowledgements**

I would like to thank my supervisors, Prof. Robert Stephen Plant and Dr. Chimene Daleu, for giving me the opportunity to study this interesting topic and providing me with the guidance in completing my project. I would also like to thank them for their advice, encourage and patience when I write this dissertation.

Furthermore, I want to thank my friends and classmates for their care and companionship. Also, thank you to my parents for giving me the support which gives me the chance to study in the University of Reading!

## Abstract

The interactions between deep convection and the large-scale circulation are the most important processes in the tropical atmosphere. We investigate the features of the response of convection to surface conditions and changes in the large-scale thermodynamic environment in this study, using Single Column Model (SCM) and parameterizing the large-scale environment by Weak Temperature Gradient (WTG) approximation.

We find that the convection is sensitive to the Sea Surface Temperature (SST) and surface wind speeds. When SST and wind speeds are larger than the reference state, the simulation of convection will develop significantly with the increase of surface flux. Meanwhile, WTG simulations show stronger sensitivity to SST. These results indicate that the surface conditions are good predictor for convection.

To study the response of convection in SCM to the changes of thermodynamic environment, we also compare the simulation with the equivalent simulation in Cloud-Resolving Model (Sessions 2015). We find deep convection is sensitive to environmental stability and moisture, while it responds more sensitively to moisture than to stability, this is contrary to study of Sessions et al. (2015) for which atmospheric stability was found to predominately affect convective activity than atmospheric moisture. And the simulated convection in moister and more stable environment can extend to tropopause in this study. Which is different from, Sessions et al. (2015) found the feature of "bottom-heavy" convection in her simulation.

On the other hand, we also find that the less stable environments inhibit convection and the more stable and moister environments produce larger precipitation, these results are similar with the results from Sessions et al. (2015).

## Table of Contents

1. Introduction .....	1
1.1 Atmospheric Convection .....	1
1.2 Interaction between Convection and Large-scale Circulation.....	3
1.3 Parameterization and Modelling.....	5
1.4 Project Motivation and Plan.....	8
2. Methodology .....	11
2.1 Single Column Model .....	11
2.2 Radiative-Convective Equilibrium State .....	12
2.3 Weak Temperature Gradient Approximation .....	13
3. Radiative-Convective Equilibrium Simulation .....	17
3.1 Experiment Design .....	17
3.2 The Analysis of RCE simulation with SST 300K .....	18
3.2.1 Time series of surface heating flux.....	18
3.2.2 Time series of total precipitation and radiative cooling.....	19
3.2.3 The anomalies of potential temperature and humidity .....	20
3.2.4 The Comparison among RCE simulations with different SSTs .....	22
4. Single Column Model Simulation with Weak Temperature Gradient.....	25
4.1 Sensitivity to the Sea Surface Temperature.....	25
4.2 Sensitivity to surface wind speed .....	30
4.3 Sensitivity to the reference profile.....	36
4.3.1 Method of perturbation .....	36
4.3.2 Effects on precipitation.....	39
4.3.3 Effects on profiles of $\theta v$ and $q$ .....	45
4.3.4 Effect on large-scale mass flux .....	47

5. Conclusion.....	49
5.1 Overview of the study.....	49
5.2 Limitations and Future Work.....	50
Bibliography.....	52

# 1. Introduction

## 1.1 Atmospheric Convection

Convection is the movement that occurs in a fluid which is caused by temperature difference. As areas are heated the fluid parcel becomes less dense than surrounded environment, and according to Archimedes principle, the parcel will experience an upward buoyancy, causing it to lift. If the parcel is cooler and its density is relatively higher, it will experience downward buoyancy, causing it to sink. Besides surface heating, atmospheric convection can also be triggered by other processes such as the convergence of surface air, the topographical lifting, and fronts.

Convection is the weather phenomenon exists widely in the atmosphere. If the Earth's surface is heated up by the sun, the near-surface air will be heated by long-wave radiation then rises. The lifting air parcel adiabatically expands and cools down, and in the presence of moisture, condensation occurs and cumulus clouds are formed and visible. Stronger convection can produce larger clouds developing with the moist air parcel rising until its buoyancy cannot balance the gravity, sometimes producing Cumulonimbus clouds and even thunderstorms.

Atmospheric convection can affect the whole troposphere even if the scale of it is relatively small. The mass and energy from the surface are able to be transported to the tropopause by convection (Plant 2015). Based on principle of mass conservation, the circulation system associated with convection must have a concentrated upward part and a surrounding downdraught part, which help to adjust the energy distribution by transporting heat away from hotter areas to cooler areas, aiding temperature circulation and reducing sharp temperature differences. Convections which have different scales lead to different energy transport: a single deep cloud that is about 1km with a circulation can only extend to 10km, but for global circulation like Hadley Cell which is composed of many cumulus clouds can extend over 100km even more. Figure 1.1 shows the delivery of energy from the surface to the upper troposphere in one cumulonimbus which is a part of Hadley Cell.

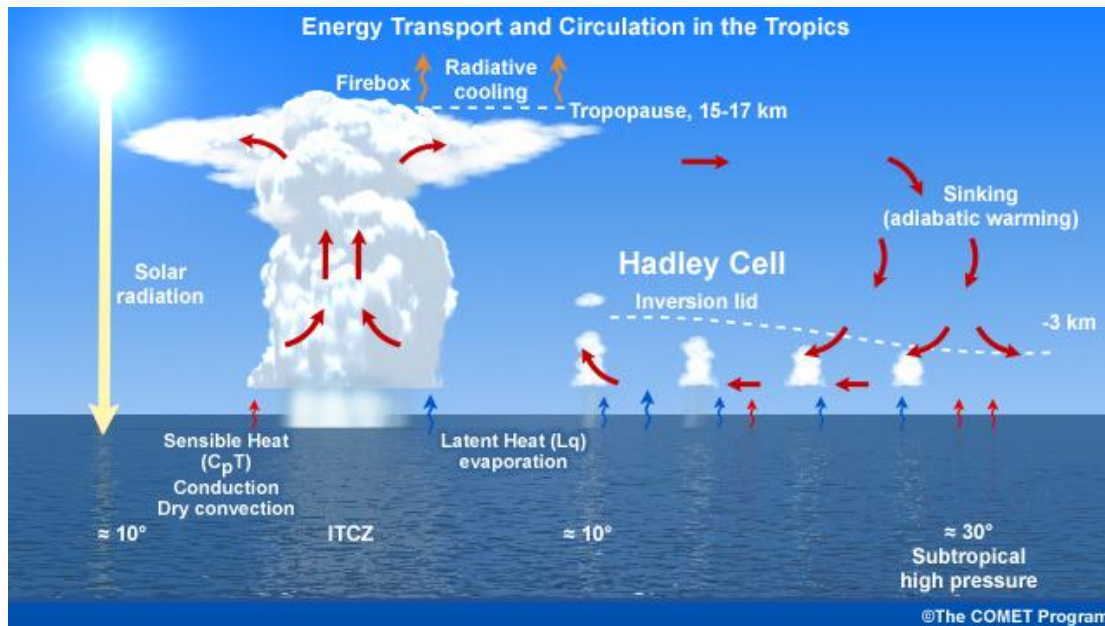


**Figure 1.1** Energy Transport and Relative Circulation in the Cumulonimbus over Tropical Ocean. ([http://ftp.comet.ucar.edu/ootw/tropical/textbook\\_2nd\\_edition/navmenu.php\\_tab\\_7\\_page\\_4.1.0.htm](http://ftp.comet.ucar.edu/ootw/tropical/textbook_2nd_edition/navmenu.php_tab_7_page_4.1.0.htm))

Buoyancy is the dominant driving force for convection, and it is highly correlated with atmospheric instability: the upward motion of an air parcel means that the atmosphere is unstable. The convective available potential energy (CAPE) can help to indicate the instability of the atmosphere. CAPE is defined by the amount of energy an air parcel releases by condensation lifting throughout a certain distance until the parcel rises to the level on which buoyancy is neutral (LNB). CAPE can provide kinetic energy for lifting. If the parcel reaches LNB, then it will get negative buoyancy. The CAPE value which is over 1000 J/kg marks the potential of deep convection like thunderstorm activity (Ambaum 2010). For the convection over the tropical western Pacific, it is found that there is sufficient CAPE for 90% of the time but only 20-30% of the time does this materialize into convective activities (Sherwood 1999), other factors like friction, entrainment and environmental compensated subsidence. On the other hand, near the relatively warmer surface, there is always a stable layer. Hence, an air parcel must overcome negative buoyancy when it begins to lift. Energy is required during the lifting process from the surface to the level of free convection (LFC). This negative energy is called Convective Inhibition (CIN).

Over some tropical areas and mid-latitude continents, the deep convection

dominates the thermodynamic structure of the atmosphere. Deep convection is related to a net release of latent heat integrated through the depth of troposphere and makes an important contribution to global precipitation (Emanuel 1994). Consequently, deep convection has important influence on dynamics and thermodynamics of the large-scale circulation. In addition to its dynamical influence on the tropical large-scale circulation, deep convection is the primary source of the upper-tropospheric water vapour and high clouds, and they both impact the radiation budget of the earth strongly. Moist air from planetary boundary layer is transported by deep convection to the dry mid- and upper troposphere, where the emitted radiation can be strongly reduced by even slight humidity change. (Shine and Sinha 1991; Spencer and Braswell 1997; Colman 2001). Therefore, it is very important to better understand the interactions between local convection and the large-scale circulation.

## **1.2 Interaction between Convection and Large-scale Circulation**

As we discussed in section 1.1, convection is the main global mechanism through which solar radiative heating of the ocean and continents is redistributed through the free atmosphere vertically. The heat input can be emitted back to space by the long-wave radiation, and the large-scale circulation is able to transport the heat as well. Furthermore, deep convection is also the main mechanism through which is a source of water vapor in upper troposphere. The upper tropospheric humidity plays a very important role in preserving the natural greenhouse effect in the atmosphere. An important and largely unsolved problem is the control of atmospheric water vapor by deep convection. The water vapor itself, as well as the strati-form clouds that are closely associated with it, has a strong influence on radiative budget and therefore on the earth's heat-driven circulation.

In regions where are experiencing deep convection, the convective clouds affect the entire depth of the troposphere and serve to link the boundary layer with the rest of the atmosphere. The convective clouds collectively affect the thermodynamic and kinematic structure of the atmosphere, which respond to and affect large-scale circulations such as tropical waves. In addition, the interaction between deep convection and large-scale flow are essential aspects of organized tropical convection as well as equatorial waves, Madden-Julia Oscillation and

monsoons.

Inside a deep convective cloud, the detrainment which occurs with the convective plume transports the moist air out to the environment, similarly the entrainment leads drier air into the convective system. Also important is the subsidence induced in the environment. Such interactions are quite complex and can be difficult to capture in convective parameterizations (e.g. Kain and Fritsch 1990, Tiedtke 1989). The shallow convection cools and moistens the atmosphere near the cloud top. But on the contrast, it warms and dries it near the cloud base. In addition, precipitation in deep cumulus that evaporates also cools and moistens the atmosphere. Deep convection also reduces entropy of the sub-cloud layer particularly by precipitation. Yanai and Esbensen (1973) combined the large-scale heating and water vapor budgets with an entrainment-detrainment model of cumulus clouds, pointed out the contribution of shallow clouds for supporting the growth of deep convection. The large-scale motion leads to a larger cloud mass flux relative to the mean vertical mass flux, which causes the compensating subsidence motion. The adiabatic compression in this downward motion produces large-scale heating, and in order to get the heat balance of environment the re-evaporation of liquid water detrained from shallow no-precipitating cumulus clouds also plays an important role.

Numerical methods can be used to analyze interaction between convection and large-scale flow. Actually, simulating both convection and the large-scale environment is very helpful to understand the process during which the convection influences the large-scale flows and environment affects it in return. For example, Posselt et al. (2012) investigated the response of deep convection to the large-scale circulation over a warming sea surface. He used a cloud-resolving model which domain is large and revealed that the increasing of atmospheric water content is sensitive to the atmospheric warming structure. Furthermore, the “large-scale rate of overturning” and convective intensity show an increasing trend of convective intensity with SST and a slowing tendency of large-scale motion.

However, to simulate the moist convection response to the evolution of the large-scale flows which includes many small processes to be considered. Various small/micro scale processes, including dynamic processes, thermodynamic

processes and microphysical processes, cannot be represented well on the relatively coarse grids used in Global Circulation Models and Global NWP. Thus, the application of parameterizations becomes necessary.

Arakawa and Schubert first proposed the quasi-equilibrium theory in 1974. It considers a statistical equilibrium between convection and large-scale environment, and could be used to evaluate aspects of feedback from convection to the large-scale circulation. If the time scale for convection is much smaller than the large-scale circulation's time scale, this quasi-equilibrium assumption is valid. To represent this effect of convective clouds in the large-scale atmosphere, the method of parameterization should be applied here.

### **1.3 Parameterization and Modelling**

In the recent decades, numerical simulation has become more and more important means of investigating the nature of atmospheric phenomena and of forecasting weather. Different Models have their individual horizontal resolution, for example, Global Circulation Models (GCMs) typically have a horizontal resolution of 50-100km, while mesoscale models have 10-50km resolution. Other higher resolution models including storm-scale models have grid sizes of the order 1-10km (Kalnay 2003). The higher resolution is supposed to describe the weather phenomenon more accurately. Thus, continuing to increase the horizontal resolution or the number of vertical layers could improve the prediction of NWP, but there are still many processes which are known as sub-grid scale processes.

The most important problem in any numerical simulation is the representation of physical processes like the turbulence motion, radiation, precipitation and other microphysics processes that occur on space and time scales too small to be explicitly calculated by the model. This presents a major challenge in the design of a model. Figure 1.2 from ECMWF website shows the time scale and spatial scale distribution of different processes, and the red lines represent the operational ECMWF model at 10km resolution, a 500m resolution so-called Cloud Resolving Model (CRM) and a 50m resolution Large Eddy Model (LEM). It is obvious that the requirements for parameterization are different for them. Usually cumulus convection clouds are around 1km in size and last about 10 minutes, which are

important for forecasting but cannot be simulated well by some coarse models.

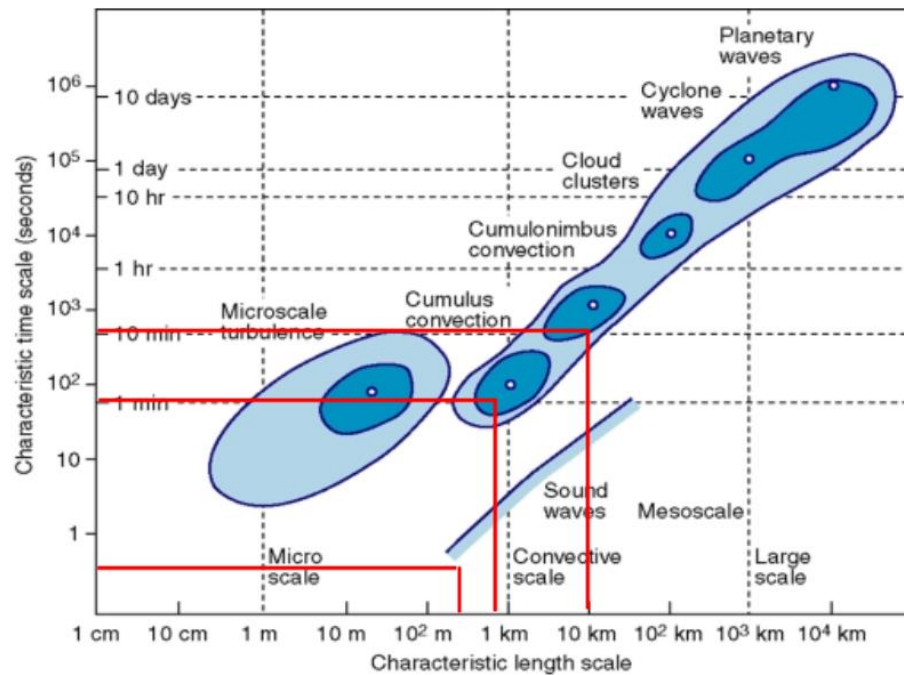


**Figure 1.2** The range of time scales on vertical axis and range of spatial scales on horizontal axis among different systems and different models represented by red lines. ([https://www.ecmwf.int/assets/elearning/parametrization/param/story\\_html5.html](https://www.ecmwf.int/assets/elearning/parametrization/param/story_html5.html))

From a mathematical aspect, finite difference equations can be used to describe the systems on scales of two or five times larger than the grid length. Parameterization is the mathematical procedure that uses prognostic variables to create empirical equations. In which the prognostic variables are used in the model equations and solved for every time step, they are predicted by the model and they describe the state of model.

Parameterized cumulus convection is very important in numerical modelling of the atmosphere, because deep convection leads to the most fundamental uncertainties and challenging problems in weather or climate prediction (Arakawa 2004). It is usually defined by the statistical effects of convection. There are several studies about the application of convective parameterizations: Slingo et al. (1996) investigated the representation of tropospheric moisture and precipitation in parameterization of convection; Grell and Freitas (2014) used a stochastic convective parameterization for air quality modelling, revealing the interaction of aerosol with evaporation of cloud drops and autoconversion of cloud

water to rain; Djotang (2010) combined different cumulus parameterization schemes to study the sensitivity in West African Monsoon simulation, and found that the rainfall due to monsoon is sensitive to the different choice of parameterization schemes. While these schemes cannot simulate the amount of precipitation accurately; Raju and Potty (2011) simulated a tropical cyclone by combining various physical parameterizations in the WRF model, the result indicates that the cyclone track, intensity and time of landfall are well simulated by using the schemes.

In order to understand the influences on each other between convection and large-scale environment and overcome the mismatch about grid scale and system scale, as we mentioned in section 1.2, convective parameterized methods could be applied. Kuo (1974) extended the cumulus convection parameterization to include both deep and shallow convection, studied the influence from convection to large-scale flow. Kuo's result showed that this formulation considers the stresses heating due to compression in descending region automatically. Randall (1989) analyzed the effect of radiatively active clouds parameterization in climate model, and found an influence of upper convective clouds related to moist convection on large-scale flows.

GCMs are relatively low-resolution models, so important sub-grid processes are parameterized, and the state-of-art GCMs are sensitive to the cumulus parameterizations (Yano et al. 1998), Lin et al. (2008) found GCMs may describe the climate variability wrongly. Large Eddy Model (LEM), are high resolution model, which can resolve the convective-scale processes explicitly like the energy transport. But an LEM cannot usually be integrated in a large enough domain to simulate the large-scale systems forcing the convection, thus, it ignores the interactions between convection with the large-scale circulation. It regards forcing as an external process which is not necessarily suitable in non-equilibrium conditions (Mapes 1997; Holloway and Neelin 2010; Masunage 2012).

Based on this, GCMs should set their resolution very high to approach the convective scale simulation and LEM must run in Cloud-Resolving Mode (CRM) on a large domain to also simulate the large-scale flow. Both of these are not realistic. To reduce the computational cost to a practical level, besides the traditional way to parameterize convection in a large-scale model, there are some new approaches.

Randall et al. (2003) chose super-parameterization, using embedded CRMs to simulate subgrid motion in a grid square; Grabowski et al, (2000) simulated large-scale flows by two-dimensional CRM; Kuang et al. (2005) rescaled the convection and large-scale circulation to reduce the scale difference, using Diabatic Acceleration and REscaling approach within a three-dimensional CRM. However, if the rescaling is too large, the life cycle length of convection may increase abnormally. Recently, some large-domain, high-resolution experiments have been performed (Holloway 2012; Liu 2009), but fundamental parameterizations of subgrid processes are still needed and the simulation are not so accurate compared with observations.

Overall, the previous studies provide us with much experience and guidance of the simulation of the interactions between convection and large-scale circulation. All of the results illustrate that a simple, efficient and accurate prediction is still necessary. Thus, this project will focus on setting up a low-computational-cost but accurate model. More description of project will be shown in section 1.4.

## **1.4 Project Motivation and Plan**

According to the studies mentioned before, the main problem is the high computational cost due to scaling mismatch between convection and large-scale circulation. One reasonable solution is using a model that reduces the amount of calculation like Single Column Model (SCM). A SCM is one column of the Global Circulation Model (GCM), which is an idealized one-dimensional model. This model must represent convective cells using a parameterization. To represent the forcing from large-scale environment in this model, a parameterization of large-scale must be applied, for example, the Weak Temperature Gradient (WTG) approximation.

In the tropics where the Coriolis force is very small, once buoyancy anomalies occurs, to maintain the nearly uniform density on isobaric surfaces, the gravity waves act to redistribute them rapidly. This leads to the weak temperature and density gradient (Daleu 2013). The WTG approximation is applied between a limited-area column and an environment state. The difference between the column and the environment drives the vertical motion, which help to reduce the

column-mean potential temperature differences within a given timescale in turn (Raymond and Zeng 2005). Thus, WTG approximation presents the feedback between convection and large-scale circulation. The details of SCM and WTG approximation will be discussed further in Chapter 2.

Therefore, this project will investigate the interaction between convection and large scale circulation using Single Column Model modified to implement the WTG approximation. The simulated column and environment interact with each other by the parameterized large-scale flows that transport the heat and moisture. The large-scale circulation is developed using a reference column configuration.

Assuming the WTG vertical velocity is zero, we can run the Single Column Model to produce a Radiative-Convective Equilibrium state with the uniform surface conditions (SST and surface wind speed). This is comparable to the large-scale state in the tropics, the RCE state means the radiative cooling rate should be balanced with the latent heating rate due to precipitation. We can then use the RCE state to define the reference column which can describe the thermodynamic profiles in the environment and provide initial conditions for WTG experiments. The reference column is assumed to be infinitely large relative to the convection column. This differs from Daleu's study (2013), which used a fully coupled two-column approach in CRMs, in which these two columns had the same area.

Studying the effects and feedback between deep convection and large-scale circulation can help us understand the tropical weather. To investigate the features of how convection respond to the environment by WTG approximation, we will explore the link with different surface conditions, and we will also studying the changes of reference profile of potential temperature and moisture, the thermodynamic environments are represented by the reference profiles (Sessions 2015). Many related studies indicate that the WTG vertical velocity is sensitive to it (Mapes 2004; Raymond and Sessions 2007; Wang and Sobel 2012). The purpose of our study is to investigate the changes of deep convection due to different environments using WTG approximation.

In this work, we will evaluate the convection response to different surface conditions and perturbed reference profiles using the WTG approach in SCM. In Sessions study (2015), a CRM was used to investigate similar experiments. We will

also compare these results from simulations performed using the SCM to those performed using CRM.

In the first part of this project we set up 50-day Radiative-Convective Equilibrium (RCE) simulations with different sea surface temperature 298K, 300K and 302K, to get different reference states. We summarize the characteristic of the air column in RCE simulations and compare the simulations with different SSTs, in particular the potential temperature and the moisture profiles.

In the second part of the project, we apply the WTG approximation and use the RCE state with SST=302K to provide initial conditions and the reference state. Simulations with the WTG approach will be run for 50 days and an average over the last 20 days will be used to define the model state at equilibrium with the WTG approach. We will examine the different adjustment of convection under different conditions, such as altering the sea surface temperature in SCM, changing the horizontal wind speed and finally changing the reference state.

Chapter 2 presents the detailed description of Single Column Model, Radiative-Convective Equilibrium and the Weak Temperature Gradient approximation; Chapter 3 focuses on the results of RCE simulations with different SSTs; Chapter 4 shows the results of the simulations with WTG approximation and Chapter 5 summarizes the conclusions of this project and discusses the project limitations and potential areas of extension to this work.

## 2. Methodology

### 2.1 Single Column Model

Single Column Model (SCM) is an idealized 1D model, which could be regarded as a single grid column of a 3D model like global model and regional model, but it is also isolated to other parts of the 3D model. There are some advantages of SCM: Firstly, SCM only represents one single air column in the numerical weather forecasting, so the amount of calculation will be reduced very significantly, the prediction could be more efficient; besides, the large-scale forcing inside the SCM is usually given by the observation, so there is no error due to dynamic or thermodynamic processes during simulation (Ghan et al. 2000; Hack et al. 2000), hence some advantages or disadvantages of parameterization schemes can be found accurately.

If the SCM is an independent column to be studied and ignoring other part of the global model, as in this project, the influence from surrounding large-scale circulation should be added by forcing term:

$$\frac{\partial \theta}{\partial t} + \mathbf{V}_h \cdot \nabla_h \theta = S_\theta - \omega \frac{\partial \theta}{\partial p} \quad (2.1a)$$

$$\frac{\partial q}{\partial t} + \mathbf{V}_h \cdot \nabla_h q = S_q - \omega \frac{\partial q}{\partial p} \quad (2.1b)$$

In these two equations, with  $\theta$  potential temperature,  $q$  specific humidity,  $p$  pressure,  $\mathbf{V}_h$  horizontal velocity,  $\omega$  vertical velocity.  $S_\theta$  and  $S_q$  are the forcing terms.  $S_\theta$  includes the radiative cooling/heating process  $Q_R$ , the convective heating  $Q_C$  and the convergence of turbulent heat fluxes  $Q_{diff}^T$ .  $S_q$  is the moisture forcing term, including the convective moisture source  $Q_q$  and the convergence of turbulent moisture fluxes  $Q_{diff}^q$  (Sobel 2000). Having these two equations, the system can be solved by two unknown variables,  $\theta$  and  $q$ . Since a SCM does not have explicit momentum or continuity equation,  $\omega$  must be specified (Sobel 2000).

The large-scale horizontal temperature/moisture gradients and the time tendencies of temperature/moisture are so small to be vanished in the tropics, so the tendency terms and horizontal advection terms could be neglected and hence

the vertical advection term could be balance with the forcing term:

$$S_\theta = Q_R + Q_C + Q_{diff}^T = \omega \frac{\partial \theta}{\partial p} \quad (2.1c)$$

$$S_q = Q_q + Q_{diff}^q = \omega \frac{\partial q}{\partial p} \quad (2.1d)$$

Thus, the surrounding environmental effect could add on the forcing term to influence the vertical motion of SCM. We will discuss this further in section 2.3.

## 2.2 Radiative-Convective Equilibrium State

The concept of Radiative-Convective Equilibrium (RCE) first developed from a radiative transfer calculation in a one-dimensional and static atmosphere (Plant et al 2015). Based on this, if the vertical profile of temperature has a stationary solution, the radiative heating/cooling rate should be zero:

$$Q_R = 0 \quad (2.2a)$$

However, this gives a wrong equilibrium state. Based on this assumption, the lapse rate in the troposphere is very sharp and may even get convectively unstable but the observed truth does not present this. Moller and Manabe (1961) even found the superadiabatic state in the atmosphere under this unrealistic full radiative equilibrium calculation. The convection should act to adjust the unstable profile to a stable one. Hence the effect from the moist convection should be added to the equation (2.2a) to modify the equilibrium state:

$$Q_R + Q_C = 0 \quad (2.2b)$$

In which  $Q_C$  is the convective heating. This convective heating in RCE arises from the surface sensible heating flux  $SH$  and latent heating flux  $LH$ :

$$SH = C_p \rho_1 C_E V_1 (SST - T_1) \quad (2.2c)$$

$$LH = L_v \rho_1 C_E V_1 (q_s(SST) - q_1) \quad (2.2d)$$

In the definition of  $SH$  and  $LH$ ,  $C_p$  is heat capacity at constant pressure,  $L_v$  is latent heat of vaporization;  $\rho_1, V_1$  and  $T_1, q_1$  are the variables at the first layer in the model, which are very close to the surface;  $C_E$  is the exchange coefficient;  $q_s(SST)$  is saturated water vapor pressure calculated by SST.

Simply speaking, the RCE describes a state in which any net loss or gain of radiative energy is balanced by the convective heating flux. Under this equilibrium

calculation, the convective heating  $Q_C$  could represent all thermodynamic and dynamic processes which are neglected within the radiative transfer calculations. Similarly, the equilibrium state of moisture within the RCE should be presented as:

$$P = E \quad (2.2e)$$

$P$  is the precipitation and  $E$  is evaporation. To get balanced in vapor budget, the amount of the moisture which condense to rainfall should equal the amount of evaporation. In practice, latent heating  $LH$  may dominates in  $Q_C$ , so the value of  $P$  must be consistent with  $LH$ . This links couples the heating component and the moisture component of RCE.

In recent studies, the notion of RCE is not only the traditional description, but refers to the final state of integrating CRM simulations over a long period, without adding any large-scale vertical motion to the models (Grabowski 2003; Cohen and Craig 2006; Stephens et al. 2008; Parodi and Emanuel 2009). Sometimes an extremely simplified method is used to compute the radiative heating/cooling rate. For example, an imposed prescribed fixed tropospheric cooling rate is applied in some convective case studies. In this project, the cooling rate will be forced as a uniform value as well, and the description of this setting will be given in Chapter 3.

When the given air column is not static anymore and a vertical motion is included, then the equilibrium state would be modified as:

$$Q_R + Q_c - \omega \frac{\partial \theta}{\partial p} = 0 \quad (2.2f)$$

$$E - P - \int \omega \frac{\partial q}{\partial p} dp = 0 \quad (2.2g)$$

Here the balanced state of heating should exist among radiative heating/cooling rate, convective heating rate and vertical advection of heating within model. Similarly, the moisture budget should consider the vertical advection of humidity as well.

### 2.3 Weak Temperature Gradient Approximation

As we mentioned briefly in section 1.4, in the tropical area, because the Coriolis force is almost zero, gravity waves can redistribute the buoyancy anomalies rapidly to maintain uniform density on isobaric surfaces. Therefore, the horizontal

gradient and time tendency of potential temperature can be very small. Figure 2.3 shows the zonal mean potential temperature profile for the global area, in which the potential temperature gradient over tropical area is seen to be very weak relative to the extra-tropics.

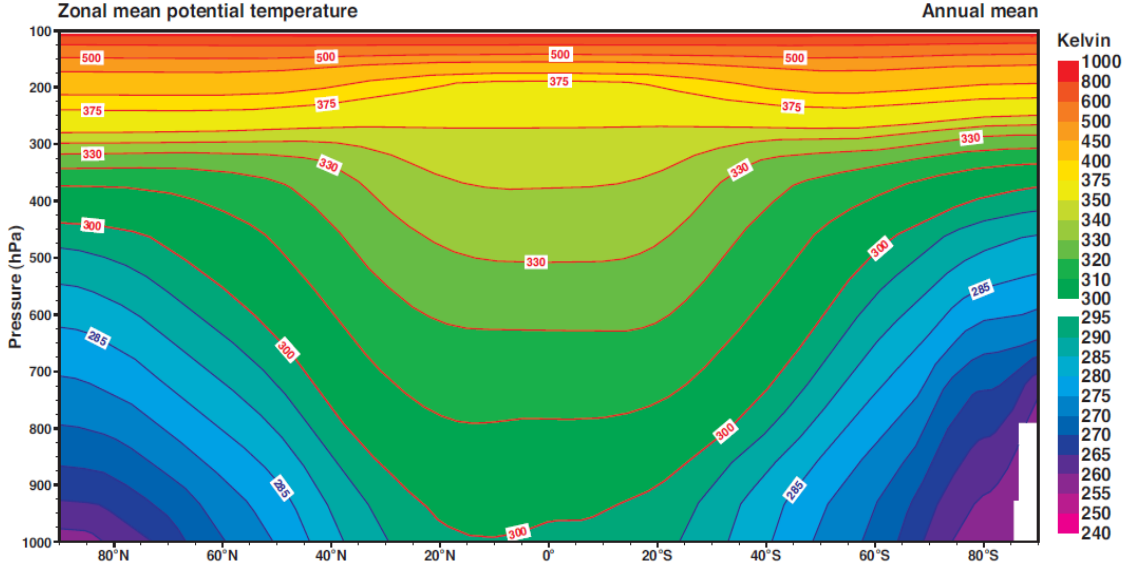


**Figure 2.3** The vertical profile of zonal mean potential temperature based on annual averaged data (Plant 2017).

Sobel and Bretherton (2000) simplified the prognostic equation for potential temperature based on the assumptions that the horizontal gradient and time tendency of  $\theta$  is weak:

$$\frac{\partial \theta}{\partial t} + \nabla_h \cdot (\mathbf{V}\theta) + \frac{1}{\rho} \frac{\partial \rho \omega \theta}{\partial p} = S_\theta \quad (2.3a)$$

They simplified to equation 2.3b, in which the diabatic heating is balanced with the vertical advection term of potential temperature:

$$\bar{\omega} \frac{\partial \bar{\theta}}{\partial p} = S_\theta \quad (2.3b)$$

The overbar represents a filtered large-scale flow. The term on the right side in equation (2.3b)  $S_\theta$  is the diabatic source term of potential temperature. This equation shows the relationship between vertical motion and environmental diabatic heating. As discussed above, the large-scale vertical velocity acts to reduce the column-mean  $\theta$  difference for maintaining the uniform temperature or density in tropics, from this idea the Weak Temperature Gradient (WTG)

approximation is developed as (Raymond and Zeng 2005):

$$\bar{\omega} \frac{\partial \bar{\theta}}{\partial p} = \frac{(\bar{\theta} - \bar{\theta}_{ref})}{\tau} \cdot F(p) \quad (2.3c)$$

$\tau$  is the relaxation timescale which is associated with the propagation of gravity waves, and  $\bar{\theta}_{ref}$  is the domain-mean potential temperature of the reference state which can represent the state of the environment.  $\bar{\theta} - \bar{\theta}_{ref}$  is potential temperature anomaly which drives the large-scale flow. Note that function  $F(p)$  is dimensionless and in Raymond and Zeng's (2005) study it is defined by " $F(p) = \sin(\pi(p_{surface} - p)/(p_{surface} - p_{tropopause}))$ ". But in this project it could be the constant one of in the paper of Wang and Sobel (2011).

The WTG approximation is not useful in boundary layer. Because there is a strong vertical mixing process inside it, vertical mixing can reduce the dynamic adjustment which is making the temperature in the free atmosphere fixed (see the 300 line in the tropical boundary layer in Fig. 2.3). Hence in boundary layer, the solution is found by interpolating the large-scale vertical flow profile linearly with height from zero on the surface to the value on the first layer above planet boundary layer (Sobel and Bretherton 2000; Raymond and Zeng 2005).

There are several applications of WTG approximation with various aspects in previous studies. Sobel and Bretherton (2000) used a SCM of a tropical quasi-equilibrium model to develop the weak temperature gradient approximation. He found that the simulated result of climatological rainfall is not dramatically different from the simulation without WTG in this model. Wang et al. (2013) studied the Madden-Julian Oscillation by using WTG simulation to incorporate the observed difference with reference profile. Sessions et al. (2015) studied the response of convection to idealized perturbations by using WTG, and revealed that stronger convection developed with more stable environments and produced higher precipitation rates than the profiles with no perturbation.

The large-scale motion  $\bar{\omega}$  can be calculated by the equation (2.3c), and using this result from large-scale parameterization, the additional heat and moisture source or sink can be simulated by:

$$\left(\frac{\partial \theta}{\partial t}\right)_{Large-scale} = -\bar{\omega} \frac{\partial \bar{\theta}}{\partial p} \quad (2.3d)$$

$$\left(\frac{\partial q}{\partial t}\right)_{Large-scale} = -\bar{\omega} \frac{\partial \bar{q}}{\partial p} + \max\left(0, \frac{\partial \bar{\omega}}{\partial p}\right) (\bar{q}_{ref} - \bar{q}) \quad (2.3e)$$

In which the terms  $\left(\frac{\partial \theta}{\partial t}\right)_{Large-scale}$  and  $\left(\frac{\partial q}{\partial t}\right)_{Large-scale}$  are adiabatic heating and moisture transport due to large-scale motion.  $\bar{q}_{ref}$  is the profile value of moisture in the reference state. The second term on the right side of equation (2.3e) represents the horizontal advection. If the vertical velocity increases with height ( $\frac{\partial \bar{\omega}}{\partial p} > 0$ ), according to continuity equation, convergent motion would occur which causes horizontal advection due to entrainment from the environment. This representation of advection have been used widely (Sessions et al. 2010; Wang et al. 2013; Herman and Raymond, 2014). As to the  $\theta$  tendency, because the horizontal gradient of potential temperature is weak in the tropics, the horizontal advection is not considered here.

Based on the equations (2.3d and 2.3e), time tendency of potential temperature and moisture due to large-scale circulation can be determined and hence we can get the value of potential temperature and specific humidity at the next time step.

### 3. Radiative-Convective Equilibrium Simulation

#### 3.1 Experiment Design

All experiments will be conducted by a SCM from UMv7.8, which is the version 7.8 of Met Office's general circulation model (Davies et al 2005). The parameter settings we used is associated with the Global Atmosphere version 3.0 (GA3.0) configuration of the atmospheric component of the HadGEM family of models (Walters et al. 2011). Gregory and Rowntree's study (1990) for convection parameterization provides the bulk mass-flux approach that we are using, with many subsequent modifications presented by Derbyshire (2011), including a smooth adaptive detrainment specification. We also use the prognostic PC2 scheme from Wilson (2008) to represent strati-form clouds, with the related microphysics following Wilson and Ballard (1999). We choose the boundary layer parameterization in the study of Lock et al. (2000).

The model is configured with 63 levels vertically, it has more accurate resolution which closer to the surface on the stretched grid. The lower boundary is an ocean surface with a prescribed time-dependent SST. The top and bottom of the model are assumed to be rigid lids. And the Coriolis parameter is set to zero. Above 15km we use a Newtonian damping layer.

Furthermore, as we discussed in section 2.2, the radiative cooling rate here has been simplified. It is set to be constant vertically with the value  $-1.5\text{K/day}$ , which is from surface to about 220hPa, and then the cooling rate decreases linearly from 220hPa until its value reaches to zero at about 120hPa. Then the radiative cooling rate is constant again with value  $0\text{K/day}$ . Figure 3.1 shows the structure of simplified radiative cooling rate. Nakajima and Matsum (1988), Isla et al. (1993) and Robe and Emanuel (1996) also used a similar radiative cooling profile in previous studies. According to observations, the mean precipitation in the tropics is about  $4.19\text{mm/day}$ , and this can be converted to be equivalent condensation warming which is about  $1.44\text{K/day}$  (Daleu 2013). Comparing this with the prescribed radiative cooling rate  $-1.5\text{K/day}$ , these two values are very similar.

Therefore, this kind of simplification is realistic.

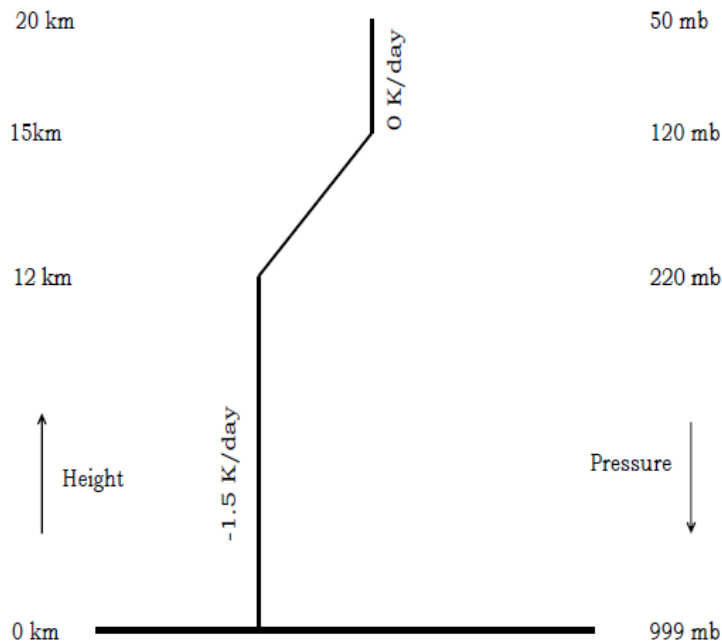


**Figure 3.1** The profile of the tropospheric cooling due to loss of the terrestrial radiation (Daleu 2015)

For the Radiative-Convective Equilibrium simulation we turn off the WTG representation of the large-scale circulation and so vertical velocity within this model is zero. We run the model for 50 days with fixed sea surface temperature 298K, 300K and 302K. We set the relaxation timescale of 3h in this experiment.

## 3.2 The Analysis of RCE simulation with SST 300K

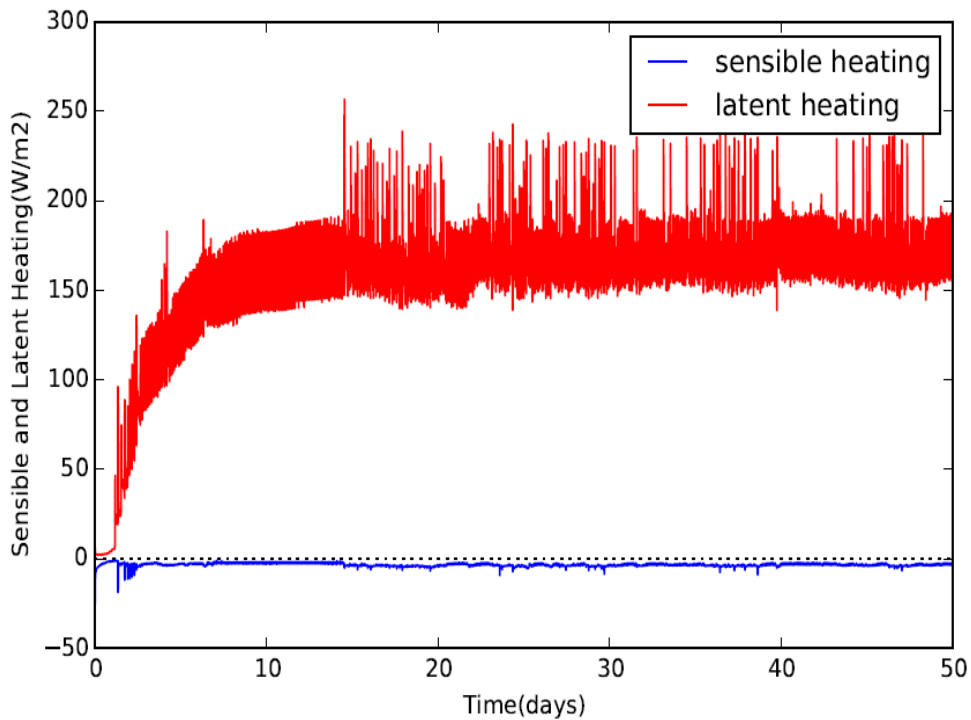
### 3.2.1 Time series of surface heating flux

Figure 3.21 shows the time series of latent heat flux which is the red line and sensible heat flux that is the blue line. Firstly the sensible heating is almost the same through the period and some very tiny fluctuations occurs. For the latent heating, the most remarkable feature is that it increases first and then becomes relatively steady from about 8<sup>th</sup> or 9<sup>th</sup> day, eventually it gets flat at the level of about  $160\text{w}/\text{m}^2$ . But there is obvious noise on the time series plot. This illustrates the occurrence and development of convection: when convection is weak, the air

column continues to cool down and the magnitude of radiative cooling is larger than convective warming due to condensation. Their difference will decrease with the development of convection. The warming balances the cooling on average but not at every time step.

Note that the absolute value of sensible heating is much smaller, therefore, latent heating dominates in this experiment. Combining some conclusions of about RCE in section 2.2 and equation (2.2b), (2.2e): radiative cooling is mainly balanced with latent heating, while latent heating is regarded as precipitation equivalently. Therefore, the main balance with the heat and moisture budget in RCE simulation must be between the radiative cooling and precipitation rate, which is:

$$Q_r + P = 0 \quad (3.2a)$$



**Figure 3.21** Time series of latent heat flux and sensible heat flux of RCE simulation with the uniform SST 300K

### 3.2.2 Time series of total precipitation and radiative cooling

Figure 3.22 compares the total precipitation rate and radiative cooling rate over the whole period. The model outputs total precipitation rate per 10 minutes, but the data is significantly discontinuous, hence we apply a one-day average to

smooth the time series here. For the time series of precipitation rate, similarly with the trend of latent heat flux, it increases at the beginning and turn to be relatively flat after about the 8<sup>th</sup> day. Fluctuations exists all the time. The time series of radiative cooling must be maintained as one value all the time because it is set artificially to a simplified constant profile before the simulation. Furthermore, the value of radiative cooling in this figure is column-integrated value and has been converted to have the same dimension as precipitation (mm/day). It is obvious that the precipitation rate over the steady state has the almost same level with radiative cooling, which indicates they are balanced in the RCE simulation.

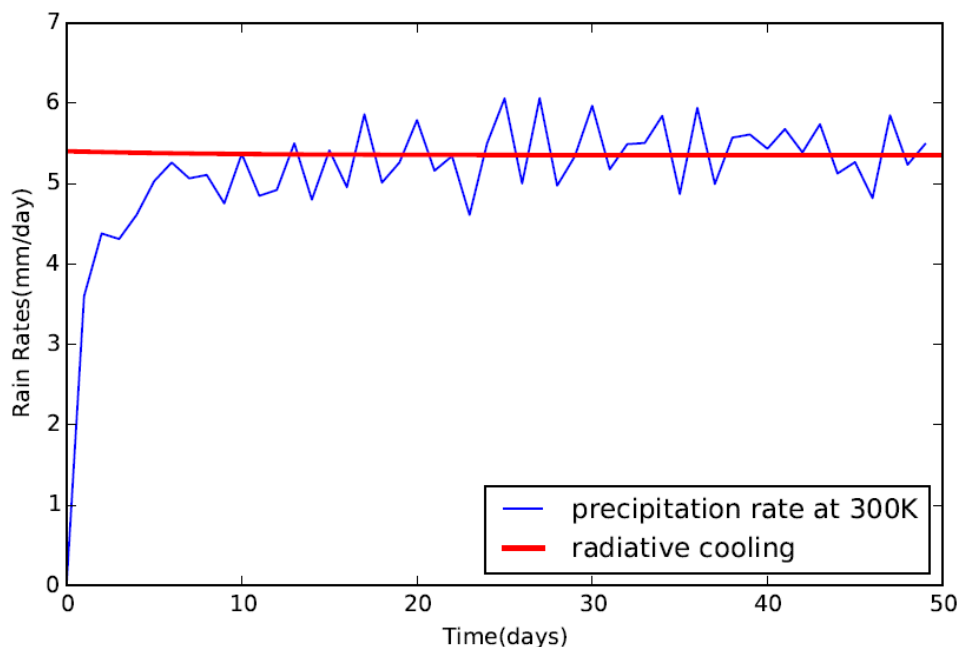


**Figure 3.22** Time series of total precipitation rate and radiative cooling of RCE simulation with the uniform SST 300K

### 3.2.3 The anomalies of potential temperature and humidity

According to the results of 3.2.1 and 3.2.2, it can be determined that the simulation will be steady from 8<sup>th</sup> or 9<sup>th</sup> day. We choose the results of the last 20-days of simulation, and calculate the average profile as reference. To show the adjustment to the equilibrium profile, we compute the anomalies for each time step and each

layer of SCM:  $\theta_t - \theta_{ref}$  and  $q_t - q_{ref}$ . Figure 3.23 shows the contour plot of potential temperature anomaly (Fig. 3.23a) and humidity anomaly (Fig. 3.23b). Based on Figure 3.23, the air column is relatively warm and humid at the beginning, the temperature and humidity is the highest at the first time step. Then the column starts to cool down which is shown in Fig. 3.23a. The potential temperature anomaly tends to be smaller and smaller in the first 30 days, and Fig. 3.23b also has the same feature. During the last 20 days, both of the anomalies are almost negligible, which represents the equilibrium state. Furthermore, the high value of potential temperature anomaly centers in the upper troposphere, and the high value of humidity anomaly locates at lower level. For the reason, evaporation occurs in the lower atmosphere so that the atmosphere would be cooled faster and moister. Moreover, the radiative cooling rate decreases in the higher troposphere and warming due to cloud formation also exists, hence the atmosphere on this layer would be warmer than lower. There is also special band at about 600hPa both in Fig. 3.23a and 3.23b, which is relatively cooler but more humid. This band is the freezing layer.

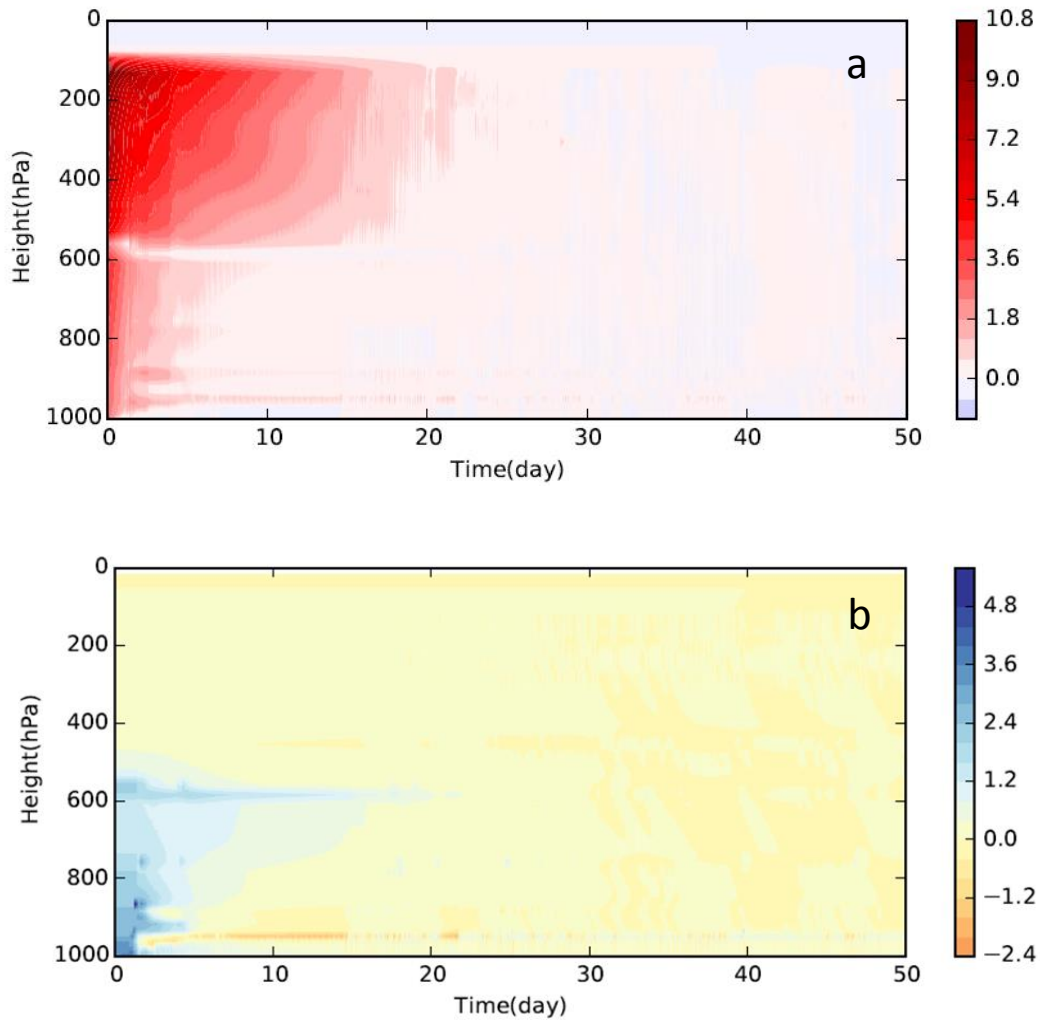


**Figure 3.23** The anomalies of potential temperature (a) and humidity (b) compared with the mean value of last 20-day results of RCE simulation with the uniform SST 300K

### 3.2.4 The Comparison among RCE simulations with different SSTs

We now make a comparison among SSTs of 298K, 300K and 302K. Figure 3.3a shows the vertical profiles of mixing ratio and 3.3b shows the potential temperature. They illustrate the general features of vertical profiles of potential temperature and humidity: the potential temperature is increasing with height and rising much more rapidly in stratosphere; the humidity is decreasing with height and the amount of water vapor is almost zero in upper troposphere and stratosphere. To compare each of the solutions, it is found that both mixing ratio and potential temperature are increasing with SST, which means high SST results in high contribution of water vapor, and even the saturation vapor pressure should be higher as well. All of this results represents the increasing evaporation. Based

on the equation (2.2e) in RCE:

$$P = E \quad (2.2e)$$

So higher SST which cause increased evaporation must lead to high precipitation simulation because precipitation is balanced with evaporation. This gets verification on the Table 1, it is very obvious that a slight increase in mean precipitation of last 20-day simulated results exists.

According to the Table 1, the mean column-integrated radiative cooling rate of last 20-day is close to the mean precipitation rate, but there is still a very tiny difference. To explain this use the equation (2.2b):

$$Q_R + Q_c = Q_R + LH + SH = 0 \quad (2.2b)$$

Where  $Q_c$  includes latent heating flux  $LH$  and sensible heat flux  $SH$ , and  $Q_R$  is radiative cooling. Latent heating due to condensation could be regarded the same as precipitation, hence the radiative cooling, total precipitation rate and latent heating flux are balanced:

$$Q_R + P + SH = 0 \quad (3.3a)$$

Figure 3.1 shows that the sensible heating flux is very weak, so  $Q_R$  could be balanced with  $P$  as we mentioned in section 3.2.1, and the small deviation between precipitation and radiative cooling in Table 1 must be sensible heating flux.

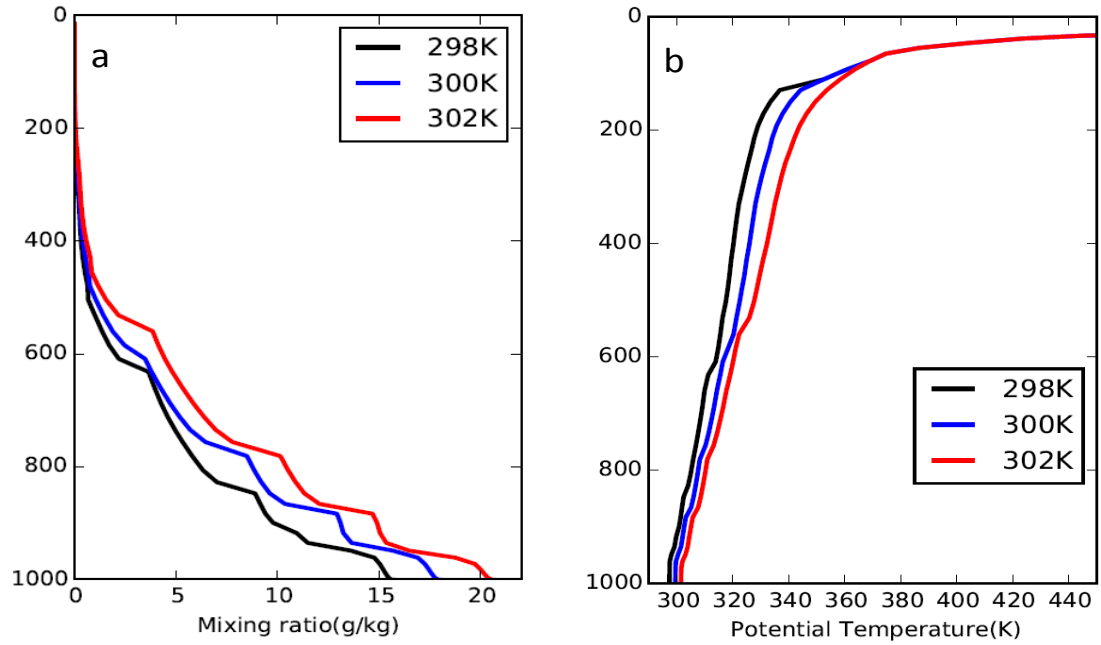


**Figure 3.3** The different vertical profiles of potential temperature (a) and humidity (b) of RCE simulation with the uniform SST 298K (black), 300K (blue) and 302K (red).

SST (K)	P (mm/day)	R (mm/day)
298	5.45028	-5.35321
300	5.49720	-5.35321
302	5.52281	-5.39231

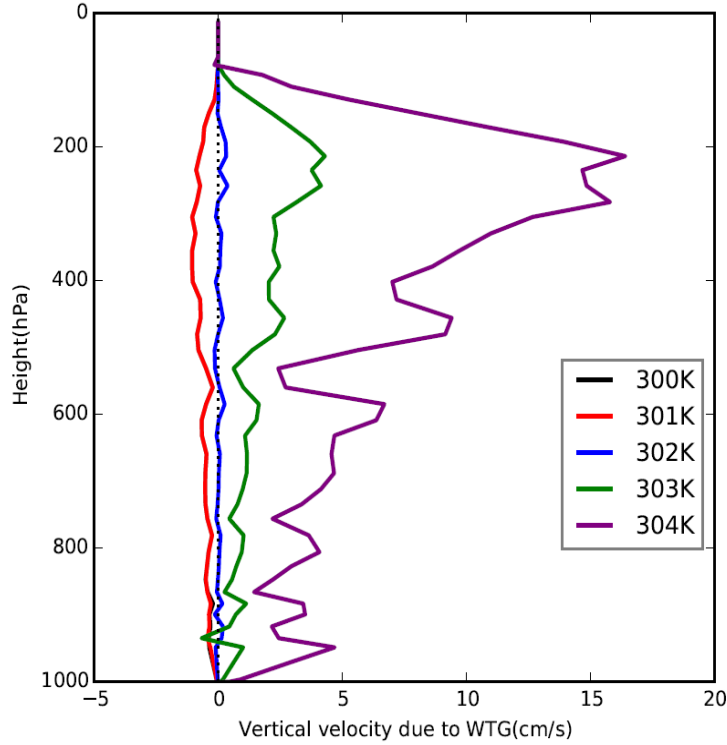
**Table 1** The values of mean precipitation rate (P) and radiative cooling rate (R) in the results of RCE simulation with the uniform SST 298K, 300K and 302K.

## 4. Single Column Model Simulation with Weak Temperature Gradient

### 4.1 Sensitivity to the Sea Surface Temperature

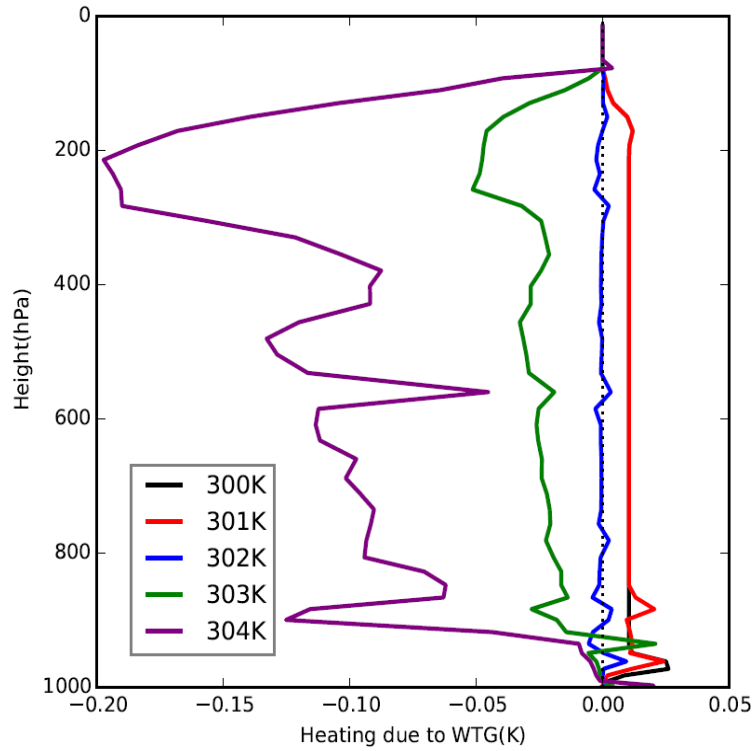
In this section, we study the sensitivity of convection to sea surface temperature using SCM modified to implement the WTG approach. We need to prescribe the reference state for the implementation of the WTG approach. This reference state is defined by the mean profiles obtained in the RCE simulation of the SCM with a uniform SST 302K and surface wind 5m/s. We conducted the WTG simulations for 50 days with different SST of 300K, 301K, 302K, 303K and 304K. Each simulation is initialized with the reference profiles. Based on the equation 2.3c, the coupling is weaker for longer relaxation timescales. We are interested in the case of strong coupling and we choose a relaxation timescale of 1h. Average the simulated results over the last 20 days to obtain the mean states and statistics at equilibrium of each simulation, the period of time that a statistical state was defined.

The equilibrium profiles of large-scale vertical velocity are shown in Figure 4.11. Generally, the total vertical velocity within column is positive when SST is larger than 302K and negative if SST is lower than 302K. The large-scale vertical velocities show a trend which increase with height until about 200hPa and then decrease. This feature is very obvious in the simulation with SST 304K (purple line), with a maximum of 15cm/s. But the maximum of vertical velocity in simulation with 302K (green line) only gets 5cm/s. The large-scale vertical velocity for the WTG simulation with SST = 302K is very close to the zero line (blue line). For the simulations with SST of 300K and 301K (black and red lines), the difference in the large-scale vertical velocities are relatively small. Therefore, the warmer surface conditions could lead to strong and active convective activity which can extent to the tropopause and the cooler condition inhibits convections. The large-scale vertical velocity simulation is very sensitive for warmer and shows relatively no change for colder SST.

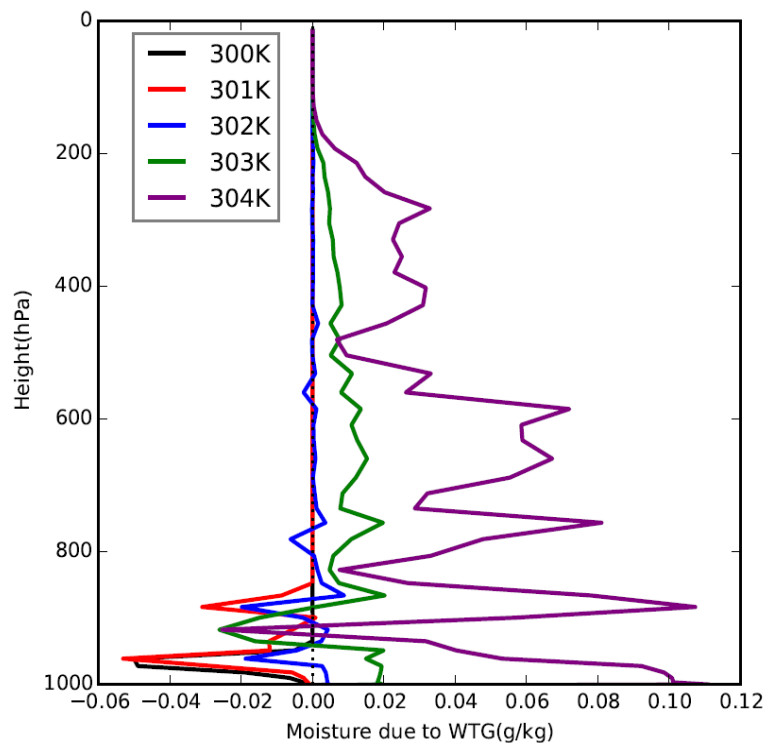


**Figure 4.11** The mean profiles of large-scale vertical velocity. Results are those obtained in the WTG simulations with different SSTs (black is 300K, red is 301K, blue is 302K, green is 303K and purple is 304K).

Figure 4.12 and Figure 4.13 show the vertical profiles of heating and moistening due to the parameterized large-scale circulation. Similarly, over uniform SST, both heating and moisture transport are close to zero, but there are some weak fluctuations in lower troposphere. For warmer SST the large-scale ascent (blue and purple curves in Figure 4.11) cools and moistens the column (blue and purple curves in Figure 4.12 and 4.13). In contrast, for cooler SST the large-scale descent warms and dries the column. This result is consistent with theory shown in Equation 2.3d, in which the adiabatic heating is negatively related to vertical velocity. For colder SST, the large-scale transport of moisture is in the lower troposphere where humidity is relatively high. For warmer SST, stronger convection transport moisture from the near surface into the free troposphere, and the large-scale  $w$  advects moisture from the reference state into the simulated column. This can be explained from the  $q$  tendency due to the large-scale vertical velocity (see equation 2.3e). The column in which  $\frac{\partial w}{\partial z} > 0$  has the convergence motion. Based on the increasing vertical speed trend illustrated in Fig. 4.11 especially the purple line,  $\frac{\partial w}{\partial z} > 0$  leads to horizontal moisture transport.



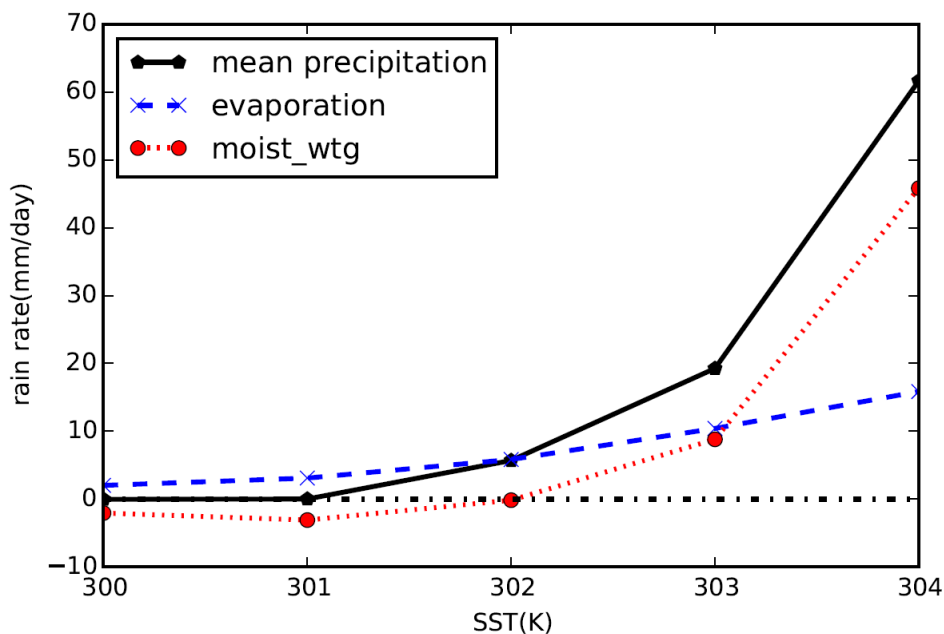
**Figure 4.12** The mean profiles of heating due to the WTG circulation. Results are those obtained in the WTG simulations with different SST conditions (black is 300K, red is 301K, blue is 302K, green is 303K and purple is 304K).



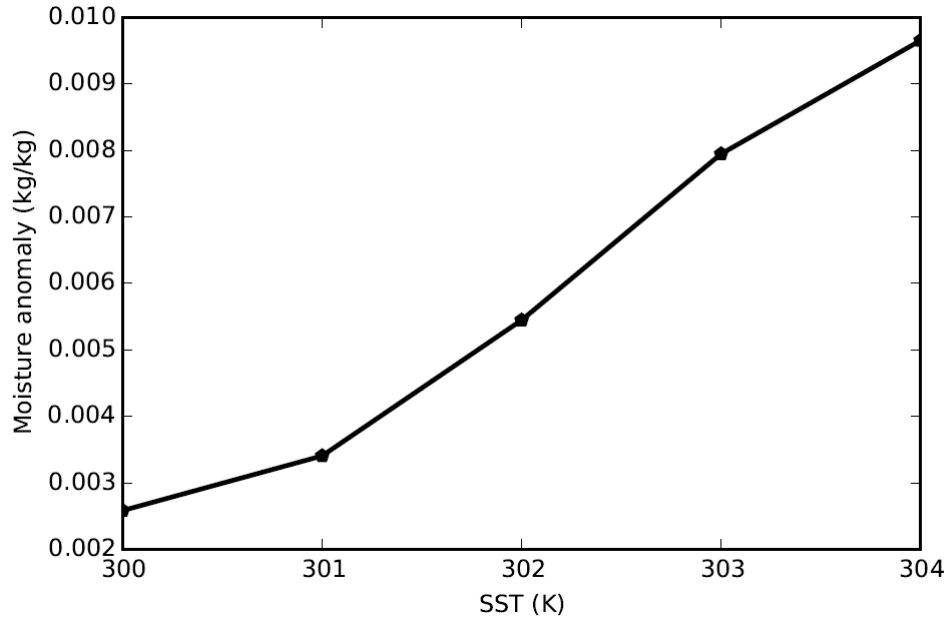
**Figure 4.13** The mean profiles of moisture due to WTG circulation. Results are those obtained in the WTG simulations with different SSTs (black is 300K, red is 301K, blue is 302K, green is 303K and purple is 304K).

Figure 4.14 shows the mean precipitation rate, evaporation and moistening rate due to the large-scale circulation results as a function of SSTs. Precipitation rate and water vapor transport show strong sensitivity to SST. When SST is 302K, which is the same SST as the reference state, the rain rate and evaporation get balanced and moisture transport is almost zero. For the same SST as the RCE reference state, the SCM under the WTG approach achieve an equilibrium state which similar to the RCE reference state. Therefore, the RCE reference state is a stable equilibrium under the WTG configuration. For the cooler columns (300K and 301K), the mean precipitation is very weak because the large-scale descent parameterized in the column inhibits the convection. However, only adding 2K from 302K could cause significantly increase rainfall.

Figure 4.15 gives a plot of saturation deficit which calculated by SST:  $q_{saturated}(SST) - q_1$ , where  $q_1$  is the mixing ratio at first model level. The increasing of saturation deficit indicates that evaporation must increase with SST, which is consistent with equation 2.2d. Precipitation rate and moistening rate show a weaker sensitivity to SST for colder SST and a stronger sensitivity for warmer SST. Evaporation changes almost linearly with the SST and its sensitivity to the SST is weaker compared to that of precipitation and moistening rate.



**Figure 4.14** Mean precipitation (black solid line), evaporation (blue dashed line) and moisture (red dotted line). Results are those obtained by averaging the last 20 days of the WTG simulations with different SSTs.



**Figure 4.15** Moisture deficit as a function of SST. Moisture deficit is calculated by  $q_{saturated}(SST) - q_1$ , where  $q_1$  is the mixing ratio at the first model level.

In the WTG simulation, the moisture budget is  $P - E = q_{wtg}$  where  $q_{wtg}$  is the moistening from the WTG circulation.  $q_{wtg}$  balances the deficit or excess of precipitation. It results in negative contribution in the cooler column but help provide water vapor in warmer column. The specific value of precipitation rate, evaporation and vapor transport shown in Table 2 can verify this. In the Table 2, the balance of heat budget ( $R + P + SH + heat_{wtg} = 0$ ) in this experiment is also proved: the sensible heating flux SH is ignored in this table because it is too small, so the value of  $R + P + heat_{wtg}$  is not precise zero. The radiative cooling rate R is a uniform value -5.4mm/day in all simulation since the cooling rate was prescribed. Precipitation P, which is regarded as heating rate from microphysics, increases with SST. The heating rate from WTG circulation in cooler column supplements the heating deficit due to lower heating from microphysics, and in warmer column it offsets the extra heat from stronger convection.

SST	300K	301K	302K	303K	304K
P	0.0	0.02	5.7	19.3	61.6
E	2.0	3.1	5.8	10.4	15.9
R	-5.4	-5.4	-5.4	-5.4	-5.4
q_wtg	-2.1	-3.1	-0.2	8.8	45.8
heat_wtg	5.5	5.5	-0.2	-13.3	-56.3

**Table 2** The values of mean precipitation rates, evaporation, radiative cooling rates, moistening rates and heating rates due to the WTG circulation. Results are those obtained by averaging the last 20 days of the WTG simulations with different SSTs (unit is mm/day).

## 4.2 Sensitivity to surface wind speed

In this section, we study the sensitivity of convection to surface wind speed by using SCM modified to implement the WTG approach. Similarly, the reference state profiles and the profiles used to initialize the WTG simulations are those in the RCE simulation with SST of 302K and surface wind of 5m/s. We conducted WTG simulation with surface wind speed of 0m/s, 3m/s, 5m/s, 6m/s, 9m/s and 12m/s. We also apply a relaxation timescale of 1h. Each simulation is performed for 50 days and the last 20 days is used to define the model state and statistic at equilibrium with the WTG approach.

Figure 4.21 shows the equilibrium profiles of the parameterized large-scale vertical velocity value. In general, vertical velocity increases from negative to positive value with surface wind speed. The simulation over the same surface wind speed as the reference state (5m/s) is equilibrium to the simulation over the uniform SST described in section 4.1. As already discussed, its vertical velocity profile fluctuates near the zero line. When surface wind increases to 6m/s (green line), the column-integrated large-scale vertical velocity shows a weak ascent in the column (result not shown). For higher surface wind speed the large-scale vertical velocity increases first with height to the tropopause and then fall to zero. This enhances convection within the column. Simulations with wind speed of 0

and 3m/s (red and black lines) show very similar profiles of large-scale vertical velocity, with small difference on the lower level. To summarize, simulations with higher surface wind speed generate large-scale ascents that enhance convection and simulation with generate large-scale descent that inhibits convection. Furthermore, based on the Fig. 4.21, the WTG simulations present high sensitivity to surface wind when the wind speed is higher than reference value.

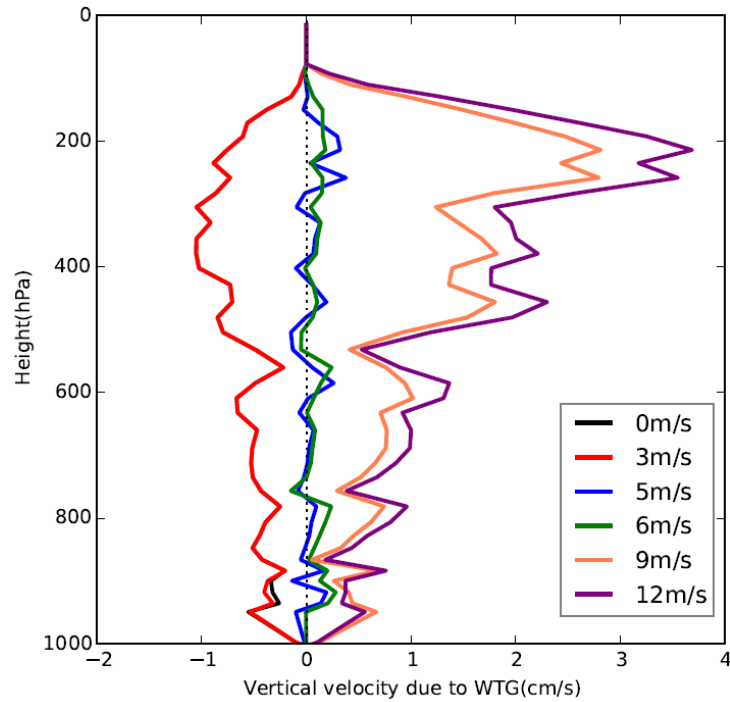


**Figure 4.21** The mean profiles of large-scale vertical velocity. Results are those obtained in the WTG simulations with different surface wind speeds (black is 0m/s, red is 3m/s, blue is 5m/s, green is 6m/s, orange is 9m/s and purple is 12m/s).

Figure 4.22 and Figure 4.23 present the vertical profiles of heating and moistening from the derived large-scale circulation. Results are shown for WTG simulations with different values of wind speeds. As discussed in section 4.1, WTG simulation over uniform surface condition produces zero mean large-scale circulation with the mean state and statistics at equilibrium which is very similar to those of the RCE reference column. Simulations with stronger surface wind speed generate large-scale ascent which cools and moistens the column while simulations with weaker surface wind speeds generate large-scale descent which warms and dries the column. Note that the heating profiles due to  $w^{wtg}$  for simulations with weaker surface wind speeds (red and black lines) have similar shapes. They are mirror image of radiative cooling (Fig. 3.1), which means the heating from the  $w^{wtg}$  offsets the radiative cooling to keep a balance of the heating budget. For simulations with weaker wind speed, the moistening due to the WTG circulation (Fig. 4.23), is centered on the lower atmosphere. It is mostly negative, corresponding to a drying as a result of subsidence inside the simulated column. For simulations with higher surface wind speed the moistening from the large-scale circulation corresponding to moistening throughout the whole column as the result of lateral entrainment from the moist environmental air and deep convection which causes moisture from the near surface into the free atmosphere.

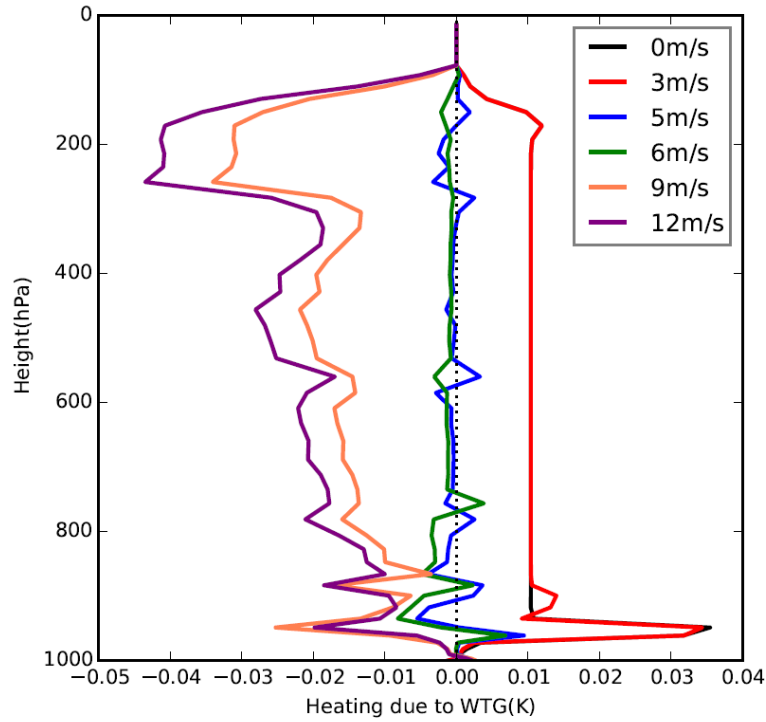


**Figure 4.22** The mean profiles of heating due to the WTG circulation. Results are those obtained in the WTG simulations with different surface wind speed conditions (black is 0m/s, red is 3m/s, blue is 5m/s, green is 6m/s, orange is 9m/s and purple is 12m/s).

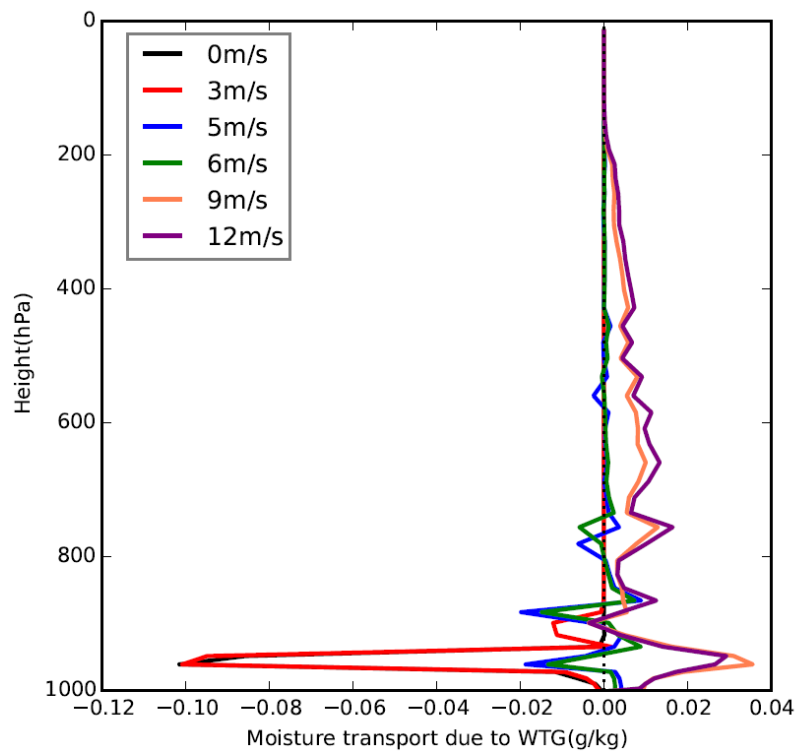


**Figure 4.23** The mean profiles of moisture due to WTG circulation. Results are those obtained in the WTG simulations with different surface wind speeds (black is 0m/s, red is 3m/s, blue is 5m/s, green is 6m/s, orange is 9m/s and purple is 12m/s).

Figure 4.24 shows the mean precipitation rate, evaporation and moisture transport from the  $w^{wtg}$ . Results are those obtained at equilibrium in the WTG simulation with different surface wind speeds. Precipitation and  $q^{wtg}$  show strong sensitivity to surface wind speed. As already discussed simulation with wind speed of 5m/s, which is the same surface condition as the reference state, it produces no mean large-scale circulation. As a result, precipitation balances evaporation and the value of  $q^{wtg}$  is zero. For simulation with weak surface wind speed, the precipitation is almost zero and  $q^{wtg}$  balances evaporation. In contrast, when surface wind speed is  $> 5\text{m/s}$ ,  $q^{wtg}$  balances the value of  $P - E$ . Evaporation increases almost linearly with surface wind speed. However precipitation rate and  $q^{wtg}$  show stronger sensitivity to surface wind speed than evaporation.

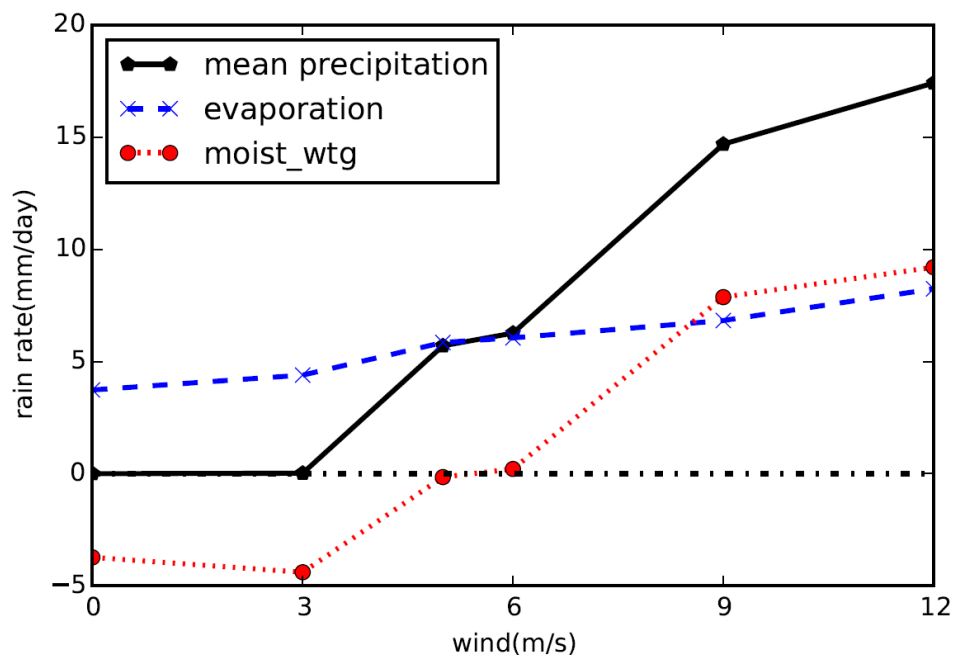


**Figure 4.24** Mean precipitation (black solid line), evaporation (blue dashed line) and moisture (red dotted line). Results are those obtained by averaging the last 20 days of the WTG simulations with different surface wind speeds.

In the simulation with the  $w^{wtg}$ , the moistening rate from the large-scale circulation balances the deficit or excess of  $P - E$ . It results in negative contribution in the column with weaker surface wind but help provide water vapor in column with stronger wind. The specific value of precipitation rate,

evaporation and vapor transport shown in Table 2 can verify this. In Table 2, the balance of heat budget ( $R + P + SH + \text{heat}_{\text{wtg}} = 0$ ) in these experiments is also proved: the sensible heating flux SH is ignored in this table because it is very small, so the value of  $R + P + \text{heat}_{\text{wtg}}$  is not exact zero. In the WTG simulations with weaker surface wind speed, the heating due to the large-scale circulation offsets radiative cooling because convection is inhibited. In the WTG simulations with stronger surface wind speed, the cooling rate from the large-scale circulation offsets the excess of heat due to stronger convection.

	0m/s	3m/s	5m/s	6m/s	9m/s	12m/s
P	0.0007	0.02	5.7	6.3	14.7	17.4
E	3.7	4.4	5.8	6.1	6.8	8.2
R	-5.4	-5.4	-5.4	-5.4	-5.4	-5.4
q_wtg	-3.7	-4.4	-0.2	0.2	7.9	9.2
heat_wtg	5.56	5.6	-0.2	-0.7	-9.1	-11.7

**Table 3** The values of mean precipitation rate, evaporation, radiative cooling rate, moisture transport due to WTG and heating rate due to WTG in the results of WTG simulation with different surface wind speeds (unit is mm/day)

From the results of section 4.1 and section 4.2, SCM simulation with the WTG approximation is sensitive to the SST or surface wind speed, especially for the more active convections. When SST or surface wind speed is larger than the RCE reference value, a large-scale ascent develops in the simulated column which enhances convection. In contrast when SST or surface wind speed is smaller than the RCE reference value, a large-scale descent develops and inhibits convection within the simulated column. The WTG simulation over uniform surface conditions showed that the RCE reference state is a stable equilibrium state under the WTG approximation. However, WTG simulations show stronger sensitivity to changes in SSTs than to changes in surface wind speeds.

## 4.3 Sensitivity to the reference profile

### 4.3.1 Method of perturbation

In section 4.1 and 4.2, we have investigated the response of convection to changes in the underlying surface conditions, when coupled to a large-scale circulation parameterized using the WTG approximation. In this section we will investigate the response of convection to changes in the thermodynamic environments. The thermodynamic environments will be changed by altering the reference potential temperature, the reference moisture or both (Emanuel et al. 2013; Herman and Raymond 2014). There are some studies about the sensitivity of convection to the changes of thermodynamic environment, in which the change in thermodynamic environment is characterized by the atmospheric stability and moisture. For example, Mapes (2004) added a vertical-dipole perturbations and vertical displacement on the  $\theta$  and  $q$  profiles to investigate the response of precipitation to them, his results indicated that the precipitation simulation is more sensitive to vertical-dipole perturbations than deep vertical displacement. Raymond and Sessions (2007) investigated the response of convection to changes in the reference environment, and found that a more stable and moist environment can cause the increase of rainfall rates for given surface fluxes. She also found that moisture perturbation only leads to change of precipitation rate without changing the shape of the profile of large-scale vertical velocity, while increasing the stability increases the vertical mass flux and decreases the level of maximum, so it can result in “bottom-heavy” convection.

Thus, to investigate the adjustment of convection simulation in different thermodynamic environment under the WTG approximation, we add the idealized perturbations to the virtual potential temperature profile and mixing ratio profile to change the reference environment, which is similar with what Raymond and Sessions (2007) did: the increase of atmospheric stability should be defined by specifying a cooling of  $\delta\theta = 4\text{K}$  centered at  $h_{low} = 3\text{km}$  and a warming of the same magnitude centered at  $h_{up} = 10\text{km}$ :

$$\Delta\theta = \delta\theta \times \left(\frac{z}{h_{low}}\right)^2 e^{\left[2\left(1-\frac{z}{h_{low}}\right)\right]} - \delta\theta \times \left(\frac{z}{h_{up}}\right)^2 e^{\left[2\left(1-\frac{z}{h_{up}}\right)\right]} \quad (4.3a)$$

In which  $z$  is the altitude. To make the reference profile less stable, we applied

perturbation of the same magnitudes but with opposite signs. (Cooling centered at 10km and warming centered at 3km). We made the reference profiles more moist (or dry) by applying a perturbation  $\delta q = +2\text{g/kg}$  (or  $\delta q = -2\text{g/kg}$ ) centered at  $h_{low}=3\text{km}$ . That is:

$$\Delta q = \delta q \times \left(\frac{z}{3km}\right)^2 e^{[2(1-\frac{z}{3km})]} \quad (4.3b)$$

This setting is similar to the drying level in the lower troposphere used by Wang and Sobel (2007). Based on the Equation 4.3a and 4.3b, we design 9 possible environments by combining all perturbations to the reference virtual potential temperature and moisture profiles. Special symbols are used to represent the environmental stability and mixing ratio perturbation (See Figure 4.31).

First, the bulls-eye is used to represent the unperturbed RCE state, which is control setting; more stable environment is represented by an upright triangle and less stable environment is an inverted triangle. A square is used to represent the neutrally stable atmosphere. Filled symbols means a moister than the reference profile. Empty symbols represent drier. Half-filled means unperturbed profile. A combined perturbations and corresponding symbols are shown in Figure 4.31:

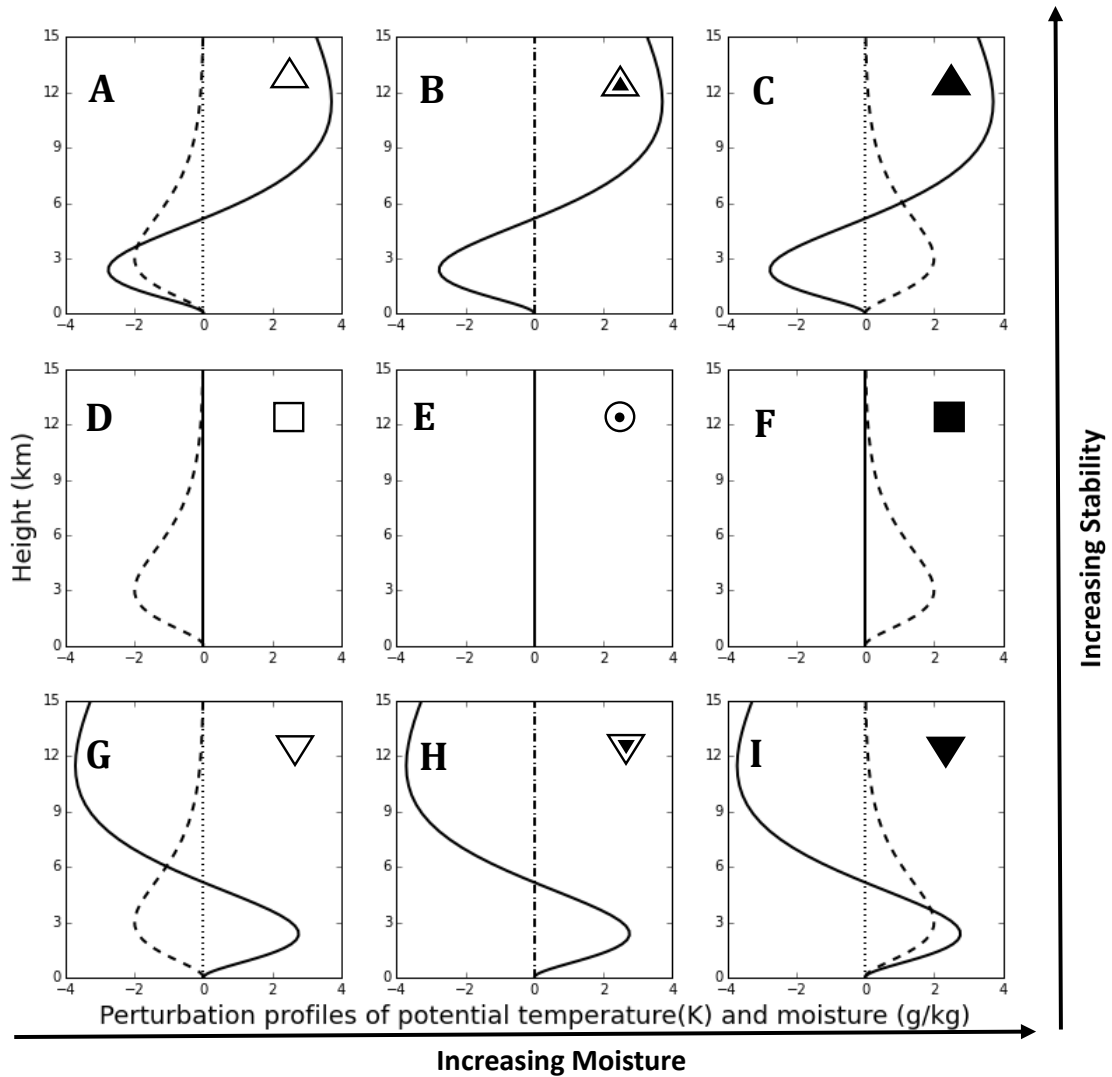


**Figure 4.31** The perturbations profiles added to the reference profile. The top row describes the more stable environments which potential temperature (solid line) is smaller in the lower and higher in the upper. The bottom row is opposite to it which represents the less stable environment. Middle row and middle column both represent unperturbed profile. And the left column is drier which moisture (dashed line) perturbation is negative, the right column is moister. The middle plot is RCE reference profile as control experiment.

Using the 9 possible environments, we design 8 experiments described in Table 4. For each experiment, we run the model for 90 days using SST of 302K and surface wind speed of 8m/s. The reference state is defined using the mean state at equilibrium of the RCE simulation with SST of 302K and surface wind speed of 5m/s. Each simulation is initialized using the reference state and relaxation timescale  $\tau = 1\text{h}$ . Provide one kind of perturbation on the environmental profile

every 30 days, and there are 2 experiments that are run with one combination of perturbation. For each experiment discussed in Table 4, the first month is unperturbed, the second month adds the perturbations on either potential temperature profile or moisture profile and the last month adds perturbations to both virtual potential temperature and moisture profiles. 30 days simulation is enough for the column to get equilibrium state after each perturbation. Average the last 10 day of each month simulation to define the mean state and statistics of the simulation with the corresponding perturbations.

	Month 1	Month 2	Month 3
Experiment 1			
Experiment 2			
Experiment 3			
Experiment 4			
Experiment 5			
Experiment 6			
Experiment 7			
Experiment 8			

**Table 4** The graphic showing the order of perturbations applied in every experiment, these symbols are the same as in Fig.4.31. The bulls-eye means unperturbed RCE profiles, triangles represent the change in stability and squares mean neutrally stable; empty symbols are drier profiles, shading means moister and half-shaded is unperturbed.

### 4.3.2 Effects on precipitation

Figure 4.32 shows the time series precipitation rate for the eight experiments. All the simulations use with unperturbed RCE profiles during the first 30 days. Days 30 to 60 represent either potential temperature or moisture perturbation, while days 60 to 90 represent both potential temperature and mixing ratio perturbation.

The perturbation method for each period has been presented by the symbol near lines. Table 5 also gives the mean values of precipitation rate, evaporation and moisture transport due to WTG circulation obtained at equilibrium of each month for the eight experiments.

Each distinct combination of reference virtual potential temperature (stabilizing/destabilizing) and or mixing ratio (drying/moistening) profiles is repeated twice (see Figure 4.32). Simulations with similar environmental conditions produce mean states and statistics which are comparable, indicating statistically similar equilibrium states.

A moister environment atmospheric stability predominately affects convection than a more stable environment. For instance, increasing the moisture by 2 g/kg produces an increase of precipitation rate of about 7.5 mm/day (with respect to the value obtained at equilibrium in the simulation with unperturbed reference state) compared to an increase of 1.9mm/day obtained in the simulations with increase in stability (compare the second month of experiments 1 and 2; 4.32 and table 5). On the other hand, a less stable environment predominately affects convection than a drier environment. As example, decreasing the moisture by 2 g/kg does not shut off, but produces a reduced precipitation due to the reduction in convective activity (empty square in Figure 4.32), while destabilizing the environment (warming of 4 K at low levels and cooling of 4 K aloft) produces a very weak precipitation rate (about 0.5 mm/day), even in a moister environment (see filled and half-filled inverted triangles in Figures 4.32). In addition, a drier, more stable environment produces precipitation which is relatively low compared to that obtained in the simulation with unperturbed reference state (compare the empty up triangle and the half-filled circle). Finally, the amount of precipitation gets increased in a moister and more stable environment compared to the unperturbed RCE profile, and compared to the simulation with increased moisture (compare the filled up triangle with the filled square and half-filled circle in Figure 4.32).

Note that the magnitudes of perturbations applied in this study are twice the values applied by Sessions (2015), whose result is shown in Figure 4.322. To study the influence to the precipitation rate from the different magnitudes of drying and moistening or stabilizing and destabilizing, we repeated the experiments 1 to 8

using the same values of perturbations as those applied by Sessions (2015). The results from those simulations are qualitatively (but not quantitatively) similar to those described above. For instance, destabilizing the environment (warming of 4 K at low levels and cooling of 4 K aloft) produces reduced precipitation rate to 0.7 mm/day (see table 5), whereas applying a warming of 2 K at low levels and cooling of 2 K aloft reduced precipitation rate to 3.4 mm/day compared to 0mm/day obtained in equivalent experiment performed by Sessions with the WTG relaxation time scale of 15 min. In this study, the WTG relaxation time scale is 1 hour and we increased the magnitudes of the perturbations in order to obtain similar convective response as in the study of Sessions. That are 4 K and 2 g/kg for the potential temperature and mixing ratio perturbations, respectively.

In this study, we showed that different choices of the magnitudes of the perturbations give qualitatively similar results and some of these results are qualitatively different from those obtained in Sessions. In contrast to our results, Sessions found larger sensitivity of precipitation to increase in stability than to increase in environmental moisture.

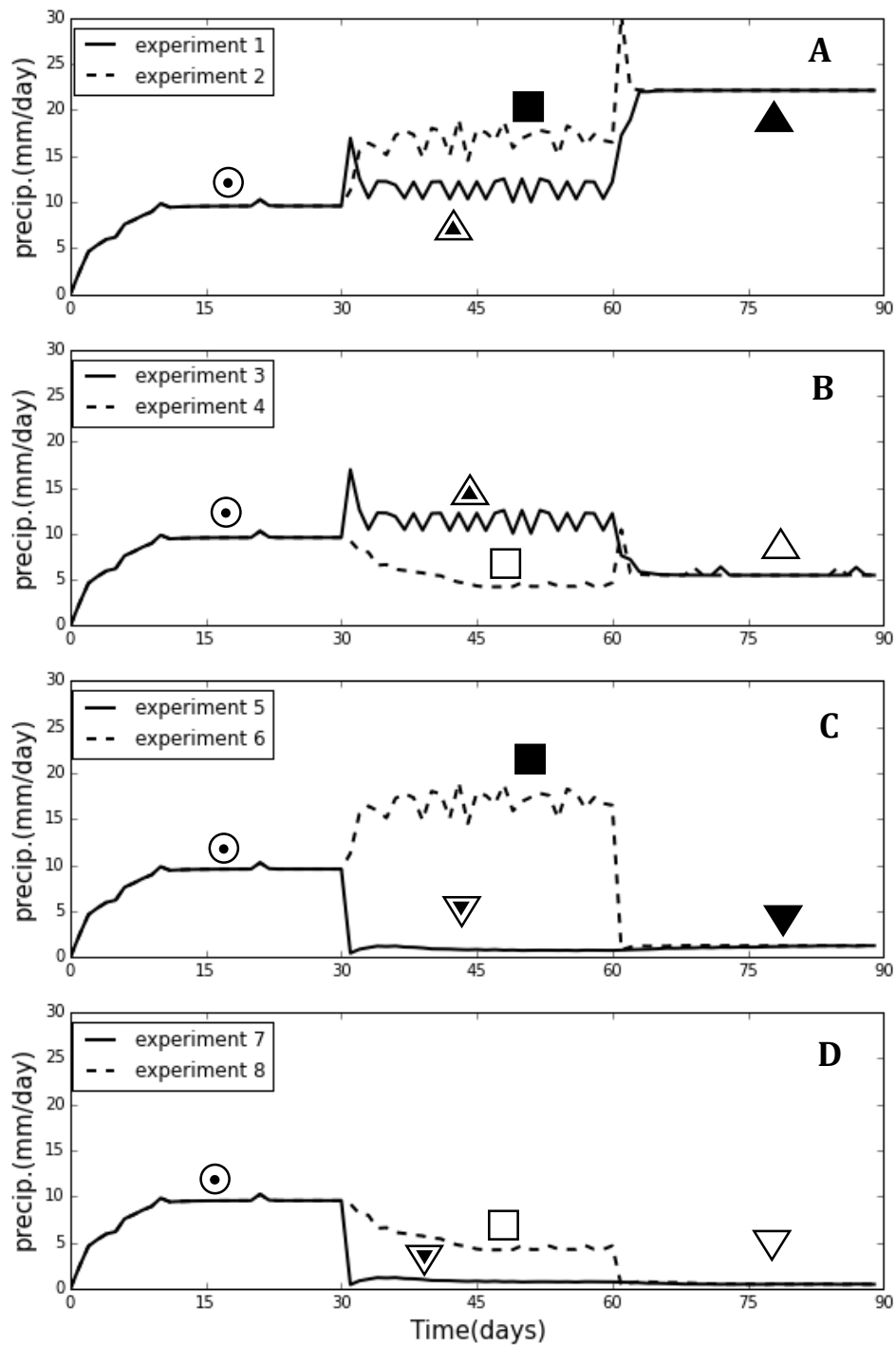


**Figure 4.32** 90 days' time series of the precipitation rate for the eight experiments. The solid lines in A, B, C, D represent experiment 1, 3, 5, 7 and the dashed lined in A, B, C, D represent experiment 2, 4, 6, 8. The perturbations of the reference state are presented by the symbols near lines.

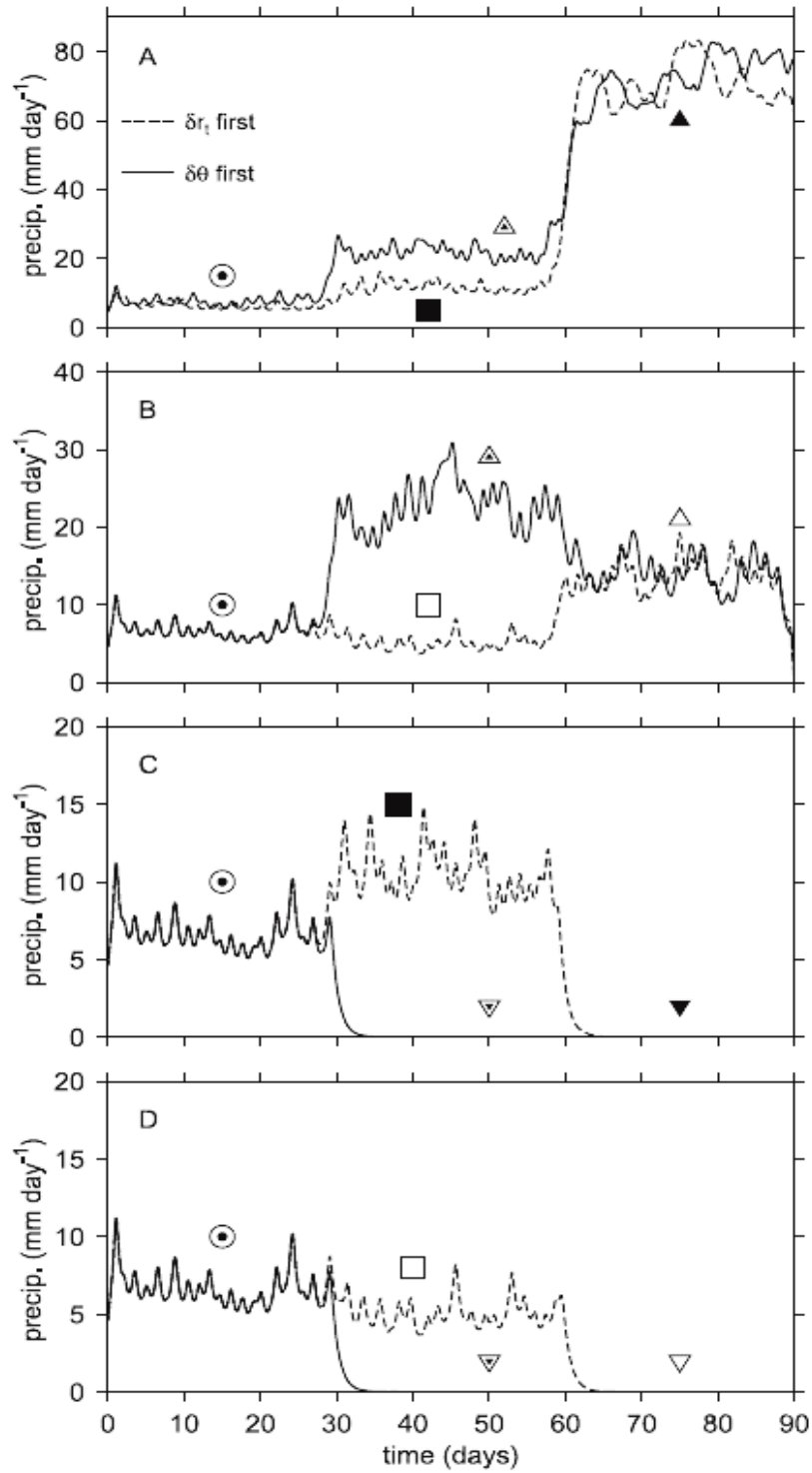


**Figure 4.322** 90 days' time series of the precipitation rate in Sharon Sessions' results (Sessions, 2015): The solid lines in A, B, C, D represent experiment 1, 3, 5, 7 and the dashed lined in A, B, C, D represent experiment 2, 4, 6, 8.

		Month 1	Month 2	Month 3
Exp 1	P	9.6 mm/day	11.5 mm/day	22.1 mm/day
	E	6.9 mm/day	10.8 mm/day	10.6 mm/day
	q_wtg	2.7 mm/day	0.6 mm/day	11.5 mm/day
Exp 2	P	9.6 mm/day	17.1 mm/day	22.1 mm/day
	E	6.9 mm/day	6 mm/day	10.6 mm/day
	q_wtg	2.7 mm/day	11.1 mm/day	11.5 mm/day
Exp 3	P	9.6 mm/day	11.5 mm/day	5.6 mm/day
	E	6.9 mm/day	10.8 mm/day	10.4 mm/day
	q_wtg	2.7 mm/day	0.6 mm/day	-4.9 mm/day
Exp 4	P	9.6 mm/day	4.4 mm/day	5.6 mm/day
	E	6.9 mm/day	7.0 mm/day	10.4 mm/day
	q_wtg	2.7 mm/day	-2.6 mm/day	-4.9 mm/day
Exp 5	P	9.6 mm/day	0.7 mm/day	1.2 mm/day
	E	6.9 mm/day	3.6 mm/day	3.4 mm/day
	q_wtg	2.7 mm/day	-2.8 mm/day	-2.1 mm/day
Exp 6	P	9.6 mm/day	17.1 mm/day	1.2 mm/day
	E	6.9 mm/day	6.0 mm/day	3.4 mm/day
	q_wtg	2.7 mm/day	11.1 mm/day	-2.1 mm/day
Exp 7	P	9.6 mm/day	0.7 mm/day	0.5 mm/day
	E	6.9 mm/day	3.6 mm/day	3.6 mm/day
	q_wtg	2.7 mm/day	-2.8 mm/day	-3.1 mm/day
Exp 8	P	9.6 mm/day	4.4 mm/day	0.5 mm/day
	E	6.9 mm/day	7 mm/day	3.6 mm/day
	q_wtg	2.7 mm/day	-2.6 mm/day	-3.1 mm/day

**Table 5** The last 10-day averaged values of precipitation rate, evaporation and moisture transport due to WTG circulation of each month for the eight experiments.

We also investigate the response of evaporation and moisture transport by the WTG-derived large-scale circulation ( $q^{wtg}$ ) to changes in the thermodynamics environment. The mean values at equilibrium for all possible changes in the thermodynamic environment (Figure 4.31) are summarized in table 5. Changes in the stability (less or more stable potential temperature) produces a larger changes in evaporation than change in moisture (compare evaporation rates in the second month of experiments 1 and 2 or experiments 7 and 8). In all cases, the moistening from the WTG-derived large-scale circulation adjusts to maintain to balance P-E.

In order to interpret the results described above, we consider Figures 4.33 and 4.34, which show the vertical profiles of  $\theta_v - \theta_{v_{ref}}$  and  $q - q_{ref}$  respectively. Those profiles are compared to the imposed perturbations (equation 4.3a and 4.3b). We also consider Figure 4.35, which shows the vertical profiles of the large-scale mass flux. The large-scale mass flux is calculated as a product of density and the large-scale vertical velocity parameterized using the WTG approximation. Results in Figures 4.33, 4.34, and 4.35 are shown for each of the possible changes in the thermodynamic environment shown in Figure 4.31.

### 4.3.3 Effects on profiles of $\theta_v$ and $q$

The shapes of  $\theta_v - \theta_{v_{ref}}$  and  $q - q_{ref}$  are similar to those obtained by Sessions (2015). A consequence of the WTG calculations is to maintain the simulated  $\theta_v$  very close to the RCE reference profile  $\theta_{v_{ref}}$ . As a result,  $\theta_v - \theta_{v_{ref}}$  is very close to the imposed perturbations profiles (Figure 4.33). The deviation is mainly located at the free atmosphere except the height near the surface ( $\sim 500\text{m}$ ) which is boundary layer. The deviation in boundary layer is because WTG approximation is not enforced in the boundary layer. In the free troposphere, the largest deviation from  $\theta_{v_{ref}}$  occurs in the environment which is more stable and moister (Figure 4.33C). For a neutral and more stable environment the deviation increases with the increase of environmental moisture (compared figure 4.33A, B and C).

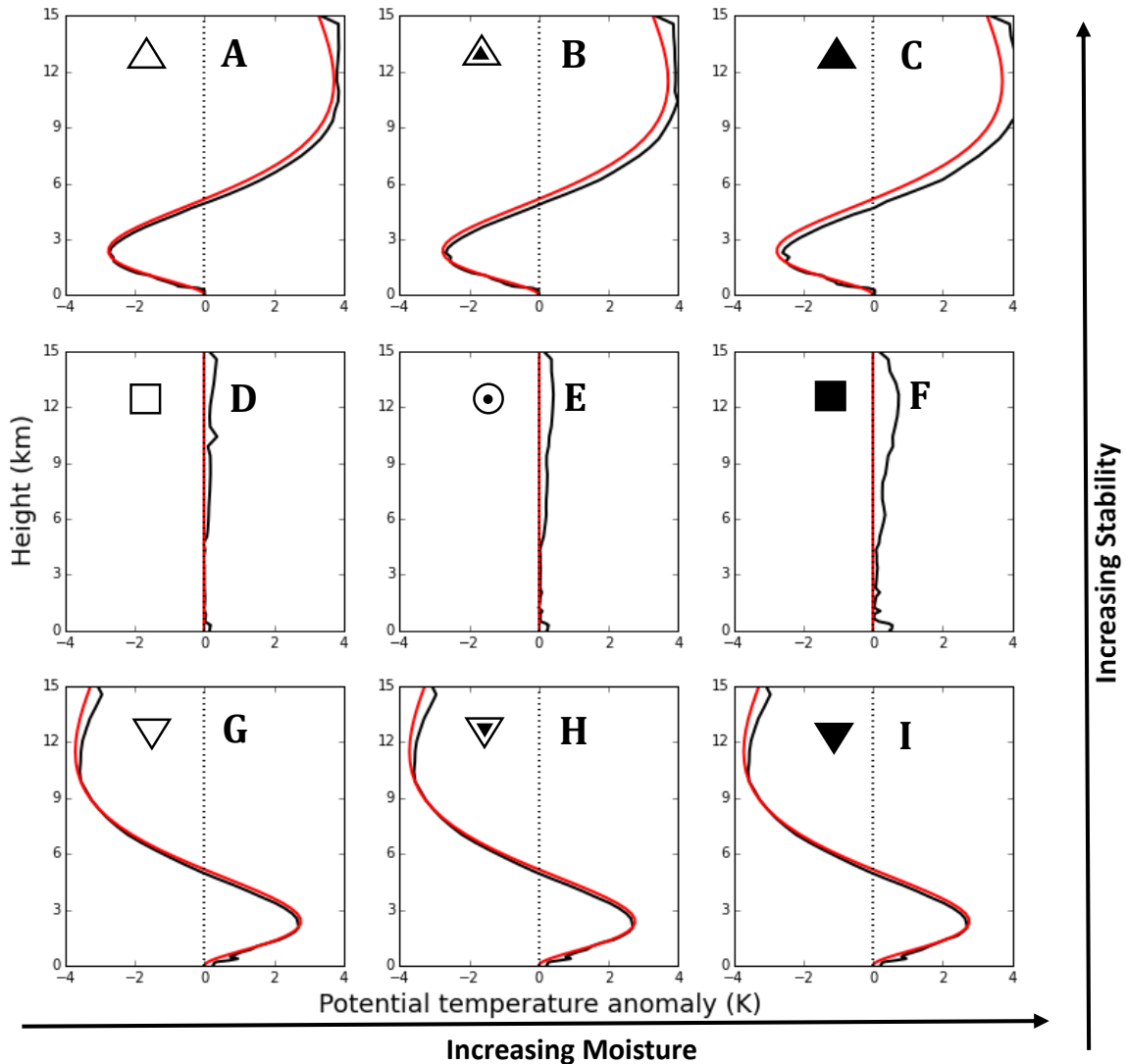


**Figure 4.33** Modeled  $\theta_v$  anomalies ( $\theta_v - \theta_{v_{ref}}$ ). Results are shown for all the possible changes in the thermodynamic environment shown on Figure 4.31.

In contrast to  $\theta_v - \theta_{v_{ref}}$ , moisture anomalies  $q - q_{ref}$  show significant differences between the profiles generated by the model compared to the imposed anomalies (compare the red and black curves in Figure 4.34). For a neutral and a more stable environment, increasing environmental moisture increases the modeled moisture (see Figure 4.34A, 4.34B and 4.34C or Figure 4.34D, 4.34E and 4.44F), and an increase in modelled moisture of up to 2.5g/kg is obtained for the moister environment (Figure 4.34F) and a more stable and moister environment (figure 4.34C). However, a less stable environment remains relatively dry (compare to the reference state), even in moister conditions (see Figure 4.34G,

4.34H and 4.34I), which is likely a consequence of the large-scale descent established in the simulated column (see Figure 4.34G, 4.35H and 4.35I).

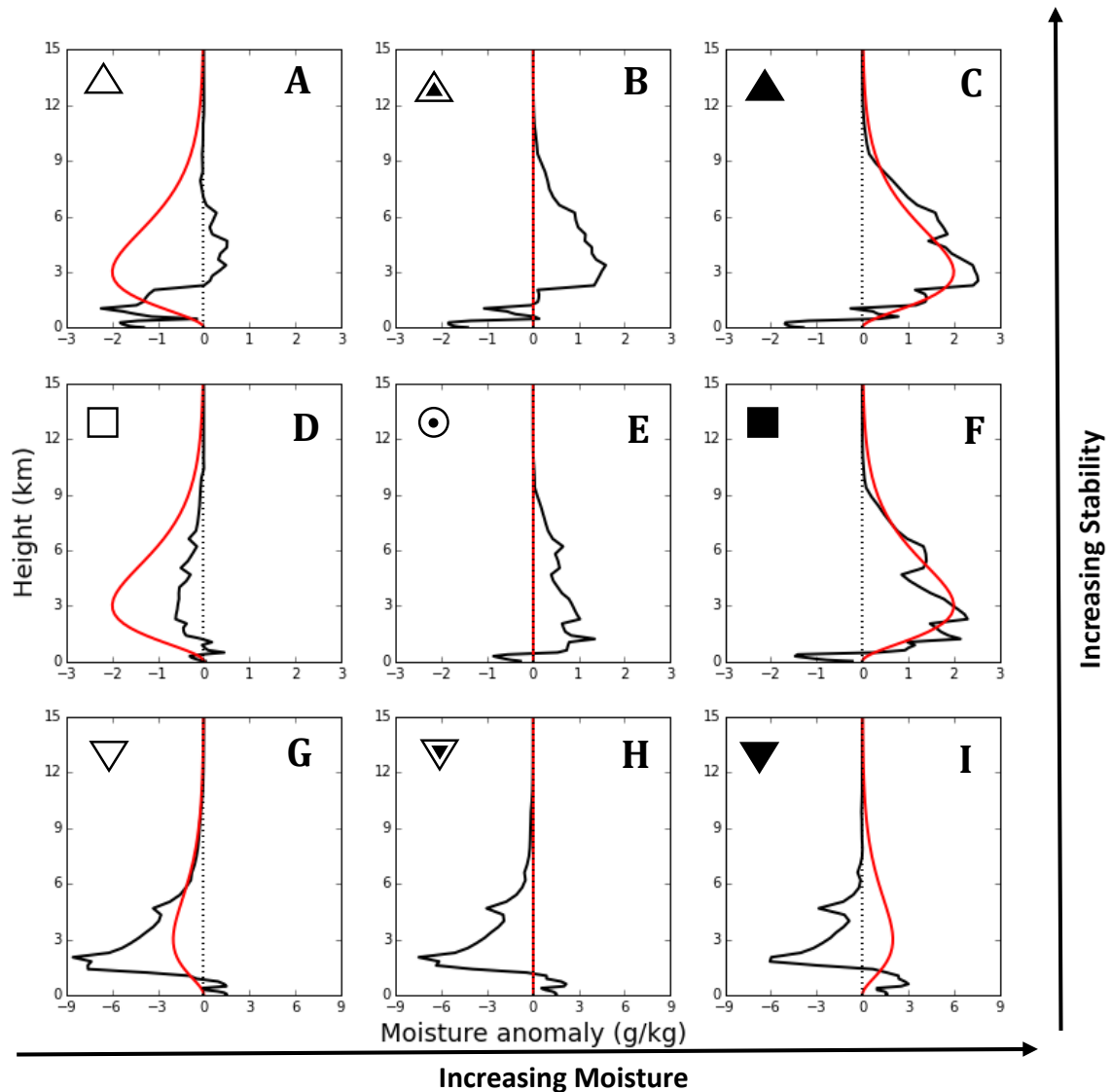


**Figure 4.34** Modeled  $q$  anomalies ( $q - q_{ref}$ ). Results are shown for all the possible changes in the thermodynamic environment shown on Figure 4.31.

#### 4.3.4 Effect on large-scale mass flux

Comparing vertical profiles of large-scale mass flux in different environments can explain the behavior of convection in these simulations. There are strongest vertical velocity in the moister and more stable environment (Figure 4.35C).

Similar to the results of Sessions (2015), a less stable environments develop a weak ascent in the boundary layer and strong decent in the free troposphere which inhibits convection event in a moister conditions. In contrast to the results of

Sessions (2015), atmospheric moisture determines the shape of the large-scale mass flux in a more stable environments, with the free tropospheric ascent extending from the lower troposphere to the tropopause as atmospheric moisture is increased (compare Figure 4.35A, B and C). Finally, atmospheric stability does not determine the shape of the large-scale vertical mass flux profile as found in Sessions (2015).

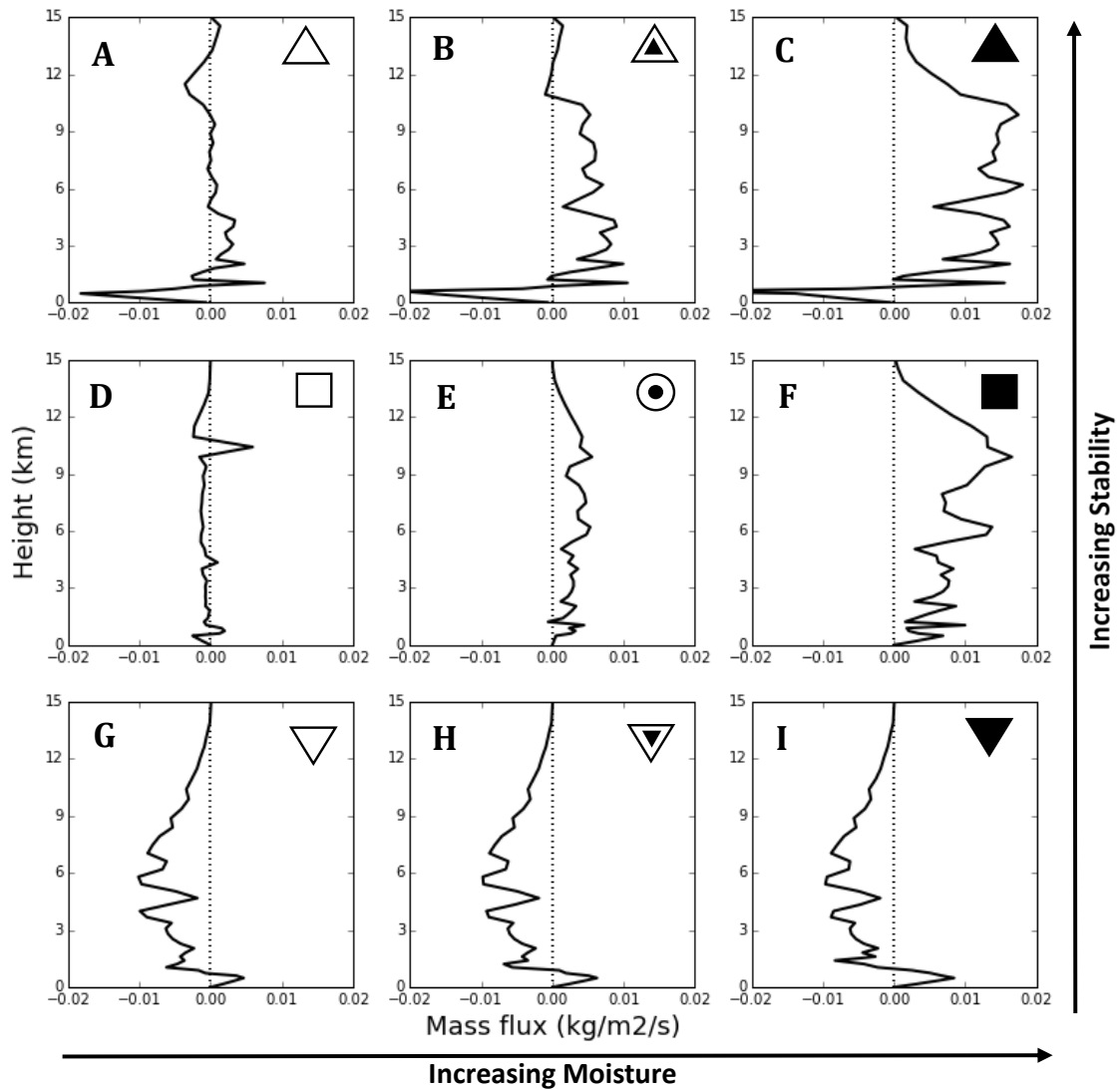


**Figure 4.35** The vertical velocity profile for each thermodynamic environmental

## 5. Conclusion

### 5.1 Overview of the study

The interactions between deep convection and the large-scale circulation are the most important processes in the tropical atmosphere. Convection transports large amounts of heat and moisture from the surface to the upper atmosphere on which they are redistributed by the large-scale flows. The heat produced by convection is an important source of energy which can drive the large-scale circulations and on the other hand the large-scale flows drive convection.

In our study, we used the SCM to investigate the features of convection respond to surface conditions and changes in the large-scale thermodynamic environment in SCM, which parameterizes large-scale environment by WTG approximation.

First, it is found that convective activity increases with Sea Surface Temperature (SST) and surface wind speeds. When SST and surface wind is larger than reference state, the simulated convection developed significantly with the increase of surface flux. Meanwhile, by comparing the results under SST condition and surface wind condition, the simulation with WTG approximation is more sensitive to SSTs, very small alteration of SST causes significant change of results. All of these simulations can maintain the heating and moisture budget balance in the column. These facts reveal that the surface conditions could be a good predictor of convection.

Using the SCM, we also investigate convective response to change in thermodynamics environment and compared our results with equivalent simulation performed using a cloud-resolving model (Sessions 2015).

For the convective response to changes in the thermodynamic environment, we found that deep convection is sensitive to both environmental stability and moisture, with atmospheric moisture leading to stronger sensitivity of convection than atmospheric stability. This results is opposite to that obtained in study of Sessions et al. (2005) for which atmospheric stability was found to predominately affect convective activity than atmospheric moisture.

Similar to the results of Sessions et al. (2015), a less stable environments inhibit precipitation convection by generating large-scale descent throughout the free

troposphere independent of the atmospheric moisture. Thus, unstable environment shuts off precipitating convection even if the environment is made moister. Besides, a moister and more stable environment produces precipitation that is greater than that produced by a stable environment as study of Sessions et al. (2015).

However, different from Sessions' investigation using a Cloud-Resolving Model (Session et al. 2015), convection is more sensitive to moisture and a stable environment generates large-scale ascent in the free troposphere with depth extending to the tropopause level for the moister case. In contrast, Session et al. (2015) found that the more stable environment produces bottom heavy convection with higher precipitation even in the moister environments. In this SCM study, the contribution of moisture in stable environment is more important. Convection is weak in more stable and drier environment, while a moister and stable environment causes very deep lifting motion which is different to the "bottom-heavy" profiles obtained in the CRM study of Sessions (2015).

The comparison of the response of convection to changes in thermodynamic environment using the Single Column Model (this study) and the Cloud-Resolving model (the study of Session et al. 2015) can help to evaluate SCM parameterized physics in a configuration in which convection is coupled to a reference reservoir column through a parameterized large-scale circulation.

## **5.2 Limitations and Future Work**

The SCM is an idealized one-dimensional model. It has low computational cost but only represents the deep convection by one vertical profile. Actually, one convective cell is a complicated three-dimensional system, one-dimensional profiles are not enough to represent the response of each part from convection to large-scale circulation. For this reason, the development of mesoscale convective systems may be eliminated and the simulation of convective systems would be unrealistic.

Furthermore, the parameterization of large-scale circulation is not only WTG approximation. Other approach include, weak-pressure gradient approach, and

spectral WTG. These other approaches can be examined in future work. On the other hand, the WTG approximation is not applied in the boundary layer and Daleu et al. (2015) showed that the results of the simulations using the WTG approximation can be sensitive to the depth of the boundary layer. Therefore, a future work could the sensitivity of the results obtained in this study the boundary layer height and also to the WTG relaxation time scale. We can also explore the response of convection to initial conditions. For example, use an artificial profile in which the mixing ratio is zero to replace the reference profile of RCE state, then investigate sensitivity of convection to dry initial conditions. Further study could also include the simulations with interactive radiation.

As future work, the experiments described here can be conducted in a set of CRMs and SCMs as in the intercomparison study of Daleu et al. (2015 and 2016).

## Bibliography

- 2018: Introduction to Tropical Meteorology, Ch. 6: Vertical Transport: 6.4 Vertical Transport in Deep Convection 6.4.1 Growth of Cumulus Clouds. *Ftp.comet.ucar.edu*, (Accessed August 7, 2018). [http://ftp.comet.ucar.edu/ootw/tropical/textbook\\_2nd\\_edition/navmenu.php\\_tab\\_7\\_page\\_4.1.0.htm](http://ftp.comet.ucar.edu/ootw/tropical/textbook_2nd_edition/navmenu.php_tab_7_page_4.1.0.htm)
- 2018: ECMWF. *ECMWF*, (Accessed August 7, 2018). <https://www.ecmwf.int/assets/elearning/>.
- Ambaum, M., 2010: *Thermal physics of the atmosphere*. Wiley-Blackwell, Hoboken, NJ,.
- Arakawa, A., and W. Schubert, 1974: Interaction of a Cumulus Cloud Ensemble with the Large-Scale Environment, Part I. *J. Atmos. Sci.*, **31**, 674-701, doi:10.1175/1520-0469(1974)031<0674:ioacce>2.0.co;2.
- Arakawa, A., 2004: The Cumulus Parameterization Problem: Past, Present, and Future. *J. Climate*, **17**, 2493-2525, doi:10.1175/1520-0442(2004)017<2493:ratcpp>2.0.co;2.
- Colman, R., 2001: On the vertical extent of atmospheric feedbacks. *Climate Dynamics*, **17**, 391-405, doi:10.1007/s003820000111.
- Cohen, B., and G. Craig, 2004: The response time of a convective cloud ensemble to a change in forcing. *Quart. Journal of the Roy. Meteor. Society*, **130**, 933-944, doi:10.1256/qj.02.218.
- Daleu, C., 2013: Simulations of interacting regions of tropical deep convection coupled by a weak-temperature gradient parameterization of the large-scale circulation. University of Reading, .
- Daleu, C. et al., 2015: Intercomparison of methods of coupling between convection and large-scale circulation: 1. Comparison over uniform surface conditions. *Journal of Advances in Modeling Earth Systems*, **7**, 1576-1601, doi:10.1002/2015ms000468.
- Daleu, C. et al., 2016: Intercomparison of methods of coupling between convection and large-scale circulation: 2. Comparison over nonuniform surface conditions. *Journal of Advances in Modeling Earth Systems*, **8**, 387-405, doi:10.1002/2015ms000570.
- Davies, T., M. Cullen, A. Malcolm, M. Mawson, A. Staniforth, A. White, and N. Wood, 2005: A new dynamical core for the Met Office's global and regional modelling of the atmosphere. *Quart. Journal of the Roy. Meteor. Society*, **131**, 1759-1782, doi:10.1256/qj.04.101.
- Derbyshire, S., A. Maidens, S. Milton, R. Stratton, and M. Willett, 2011: Adaptive detrainment in a convective parametrization. *Quart. Journal of the Roy. Meteor. Society*, **137**, 1856-1871, doi:10.1002/qj.875.

- Emanuel, K., 1994: *Atmospheric convection*. Oxford University Press, Oxford,.
- Emanuel, K., and A. Sobel, 2013: Response of tropical sea surface temperature, precipitation, and tropical cyclone-related variables to changes in global and local forcing. *Journal of Advances in Modeling Earth Systems*, **5**, 447-458, doi:10.1002/jame.20032.
- Ghan, S. et al., 2000: A comparison of single column model simulations of summertime midlatitude continental convection. *Journal of Geophysical Research: Atmospheres*, **105**, 2091-2124, doi:10.1029/1999jd900971.
- Grabowski, W., J. Yano, and M. Moncrieff, 2000: Cloud Resolving Modeling of Tropical Circulations Driven by Large-Scale SST Gradients. *J. Atmos. Sci.*, **57**, 2022-2040, doi:10.1175/1520-0469(2000)057<2022:crmotc>2.0.co;2.
- Grabowski, W., 2003: Impact of Cloud Microphysics on Convective–Radiative Quasi Equilibrium Revealed by Cloud-Resolving Convection Parameterization. *J. Climate*, **16**, 3463-3475, doi:10.1175/1520-0442(2003)016<3463:iocmoc>2.0.co;2.
- Gregory, D., and P. Rowntree, 1990: A Mass Flux Convection Scheme with Representation of Cloud Ensemble Characteristics and Stability-Dependent Closure. *Mon. Wea. Rev.*, **118**, 1483-1506, doi:10.1175/1520-0493(1990)118<1483:amfcsw>2.0.co;2.
- Grell, G., and S. Freitas, 2014: A scale and aerosol aware stochastic convective parameterization for weather and air quality modeling. *Atmospheric Chemistry and Physics*, **14**, 5233-5250, doi:10.5194/acp-14-5233-2014.
- Hack, J., and J. Pedretti, 2000: Assessment of Solution Uncertainties in Single-Column Modeling Frameworks. *J. Climate*, **13**, 352-365, doi:10.1175/1520-0442(2000)013<0352:aosuis>2.0.co;2.
- Herman, M., and D. Raymond, 2014: WTG cloud modeling with spectral decomposition of heating. *Journal of Advances in Modeling Earth Systems*, **6**, 1121-1140, doi:10.1002/2014ms000359.
- Holloway, C., and J. Neelin, 2010: Temporal Relations of Column Water Vapor and Tropical Precipitation. *J. Atmos. Sci.*, **67**, 1091-1105, doi:10.1175/2009jas3284.1.
- Holloway, C., S. Woolnough, and G. Lister, 2012: Precipitation distributions for explicit versus parametrized convection in a large-domain high-resolution tropical case study. *Quart. Journal of the Roy. Meteor. Society*, **138**, 1692-1708, doi:10.1002/qj.1903.
- Islam, S., R. Bras, and K. Emanuel, 1993: Predictability of Mesoscale Rainfall in the Tropics. *Journal of Applied Meteorology*, **32**, 297-310, doi:10.1175/1520-0450(1993)032<0297:pomrit>2.0.co;2.
- Kain, J., and J. Fritsch, 1990: A One-Dimensional Entraining/Detraining Plume Model and Its Application in Convective Parameterization. *J. Atmos. Sci.*, **47**, 2784-2802, doi:10.1175/1520-0469(1990)047<2784:aodepm>2.0.co;2.

- Kalnay, E., 2003: *Atmospheric modeling, data assimilation, and predictability*. Cambridge University Press, Cambridge, U.K.,
- Kuang, Z., 2005: A new approach for 3D cloud-resolving simulations of large-scale atmospheric circulation. *Geophysical Research Letters*, **32**, doi:10.1029/2004gl021024.
- Kuo, H., 1974: Further Studies of the Parameterization of the Influence of Cumulus Convection on Large-Scale Flow. *J. Atmos. Sci.*, **31**, 1232-1240, doi:10.1175/1520-0469(1974)031<1232:fsotpo>2.0.co;2.
- Lin, J., M. Lee, D. Kim, I. Kang, and D. Frierson, 2008: The Impacts of Convective Parameterization and Moisture Triggering on AGCM-Simulated Convectively Coupled Equatorial Waves. *J. Climate*, **21**, 883-909, doi:10.1175/2007jcli1790.1.
- Liu, P. et al., 2009: An MJO Simulated by the NICAM at 14- and 7-km Resolutions. *Mon. Wea. Rev.*, **137**, 3254-3268, doi:10.1175/2009mwr2965.1.
- Lock, A., A. Brown, M. Bush, G. Martin, and R. Smith, 2000: A New Boundary Layer Mixing Scheme. Part I: Scheme Description and Single-Column Model Tests. *Mon. Wea. Rev.*, **128**, 3187-3199, doi:10.1175/1520-0493(2000)128<3187:anblms>2.0.co;2.
- Mapes, B., 1997: Equilibrium Vs. Activation Control of Large-Scale Variations of Tropical Deep Convection. *The Physics and Parameterization of Moist Atmospheric Convection*, 321-358, doi:10.1007/978-94-015-8828-7\_13.
- Mapes, B., 2004: Sensitivities of Cumulus-Ensemble Rainfall in a Cloud-Resolving Model with Parameterized Large-Scale Dynamics. *J. Atmos. Sci.*, **61**, 2308-2317, doi:10.1175/1520-0469(2004)061<2308:socria>2.0.co;2.
- Masunaga, H., 2012: A Satellite Study of the Atmospheric Forcing and Response to Moist Convection over Tropical and Subtropical Oceans. *J. Atmos. Sci.*, **69**, 150-167, doi:10.1175/jas-d-11-016.1.
- Moller, F., and S. Manabe, 1961: Über das Strahlungsgleichgewicht der Atmosphäre. *Z. Meteor.*, **15**, 3-8.
- Nakajima, K., and T. Matsuno, 1988: Numerical Experiments Concerning the Origin of Cloud Clusters in the Tropical Atmosphere. *Journal of the Meteor. Society of Japan. Ser. II*, **66**, 309-329, doi:10.2151/jmsj1965.66.2\_309.
- Parodi, A., and K. Emanuel, 2009: A Theory for Buoyancy and Velocity Scales in Deep Moist Convection. *J. Atmos. Sci.*, **66**, 3449-3463, doi:10.1175/2009jas3103.1.
- Plant, R., and J. Yano, *Parameterization of atmospheric convection*.
- Posselt, D., S. Heever, G. Stephens, and M. Igel, 2012: Changes in the Interaction between Tropical Convection, Radiation, and the Large-Scale Circulation in a Warming Environment. *J. Climate*, **25**, 557-571, doi:10.1175/2011jcli4167.1.

- Raju, P., J. Potty, and U. Mohanty, 2011: Sensitivity of physical parameterizations on prediction of tropical cyclone Nargis over the Bay of Bengal using WRF model. *Meteorology and Atmospheric Physics*, **113**, 125-137, doi:10.1007/s00703-011-0151-y.
- Randall, D., Harshvardhan, D. Dazlich, and T. Corsetti, 1989: Interactions among Radiation, Convection, and Large-Scale Dynamics in a General Circulation Model. *J. Atmos. Sci.*, **46**, 1943-1970, doi:10.1175/1520-0469(1989)046<1943:iarcal>2.0.co;2.
- Randall, D., M. Khairoutdinov, A. Arakawa, and W. Grabowski, 2003: Breaking the Cloud Parameterization Deadlock. *Bull. Amer. Meteor. Soc.*, **84**, 1547-1564, doi:10.1175/bams-84-11-1547.
- Raymond, D., and X. Zeng, 2000: Instability and large-scale circulations in a two-column model of the tropical troposphere. *Quart. Journal of the Roy. Meteor. Society*, **126**, 3117-3135, doi:10.1002/qj.49712657007.
- Raymond, D., and X. Zeng, 2005: Modelling tropical atmospheric convection in the context of the weak temperature gradient approximation. *Quart. Journal of the Roy. Meteor. Society*, **131**, 1301-1320, doi:10.1256/qj.03.97.
- Raymond, D., and S. Sessions, 2007: Evolution of convection during tropical cyclogenesis. *Geophysical Research Letters*, **34**, doi:10.1029/2006gl028607.
- Robe, F., and K. Emanuel, 1996: Moist Convective Scaling: Some Inferences from Three-Dimensional Cloud Ensemble Simulations. *J. Atmos. Sci.*, **53**, 3265-3275, doi:10.1175/1520-0469(1996)053<3265:mcssif>2.0.co;2.
- Sessions, S., S. Sugaya, D. Raymond, and A. Sobel, 2010: Multiple equilibria in a cloud-resolving model using the weak temperature gradient approximation. *Journal of Geophysical Research*, **115**, doi:10.1029/2009jd013376.
- Sessions, S., M. Herman, and S. Sentić, 2015: Convective response to changes in the thermodynamic environment in idealized weak temperature gradient simulations. *Journal of Advances in Modeling Earth Systems*, **7**, 712-738, doi:10.1002/2015ms000446.
- Sherwood, S., 1999: Convective Precursors and Predictability in the Tropical Western Pacific. *Mon. Wea. Rev.*, **127**, 2977-2991, doi:10.1175/1520-0493(1999)127<2977:cpapit>2.0.co;2.
- Shine, K., and A. Sinha, 1991: Sensitivity of the Earth's climate to height-dependent changes in the water vapour mixing ratio. *Nature*, **354**, 382-384, doi:10.1038/354382a0.
- Slingo, J. et al., 1996: Intraseasonal oscillations in 15 atmospheric general circulation models: results from an AMIP diagnostic subproject. *Climate Dynamics*, **12**, 325-357, doi:10.1007/s003820050112.

- Sobel, A., and C. Bretherton, 2000: Modeling Tropical Precipitation in a Single Column. *J. Climate*, **13**, 4378-4392, doi:10.1175/1520-0442(2000)013<4378:mtpias>2.0.co;2.
- Spencer, R., and W. Braswell, 1997: How Dry is the Tropical Free Troposphere? Implications for Global Warming Theory. *Bull. Amer. Meteor. Soc.*, **78**, 1097-1106, doi:10.1175/1520-0477(1997)078<1097:hdittf>2.0.co;2.
- Stephens, G., S. van den Heever, and L. Pakula, 2008: Radiative–Convective Feedbacks in Idealized States of Radiative–Convective Equilibrium. *J. Atmos. Sci.*, **65**, 3899-3916, doi:10.1175/2008jas2524.1.
- Tchotchou, L., and F. Kamga, 2009: Sensitivity of the simulated African monsoon of summers 1993 and 1999 to convective parameterization schemes in RegCM3. *Theoretical and Applied Climatology*, **100**, 207-220, doi:10.1007/s00704-009-0181-2.
- Tiedtke, M., 1989: A Comprehensive Mass Flux Scheme for Cumulus Parameterization in Large-Scale Models. *Mon. Wea. Rev.*, **117**, 1779-1800, doi:10.1175/1520-0493(1989)117<1779:acmfsf>2.0.co;2.
- Wang, S., and A. Sobel, 2011: Response of convection to relative sea surface temperature: Cloud-resolving simulations in two and three dimensions. *Journal of Geophysical Research*, **116**, doi:10.1029/2010jd015347.
- Wang, S., and A. Sobel, 2012: Impact of imposed drying on deep convection in a cloud-resolving model. *Journal of Geophysical Research: Atmospheres*, **117**, n/a-n/a, doi:10.1029/2011jd016847.
- Wang, S., A. Sobel, and Z. Kuang, 2013: Cloud-resolving simulation of TOGA-COARE using parameterized large-scale dynamics. *Journal of Geophysical Research: Atmospheres*, **118**, 6290-6301, doi:10.1002/jgrd.50510.
- Walters, D. et al., 2013: The Met Office Unified Model Global Atmosphere 4.0 and JULES Global Land 4.0 configurations. *Geoscientific Model Development Discussions*, **6**, 2813-2881, doi:10.5194/gmdd-6-2813-2013.
- Wilson, D., A. Bushell, A. Kerr-Munslow, J. Price, and C. Morcrette, 2008: PC2: A prognostic cloud fraction and condensation scheme. I: Scheme description. *Quart. Journal of the Roy. Meteor. Society*, **134**, 2093-2107, doi:10.1002/qj.333.
- Wilson, D., and S. Ballard, 1999: A microphysically based precipitation scheme for the UK Meteorological office unified model. *Quart. Journal of the Roy. Meteor. Society*, **125**, 1607-1636, doi:10.1002/qj.49712555707.
- Yanai, M., S. Esbensen, and J. Chu, 1973: Determination of Bulk Properties of Tropical Cloud Clusters from Large-Scale Heat and Moisture Budgets. *J. Atmos. Sci.*, **30**, 611-627, doi:10.1175/1520-0469(1973)030<0611:dobpot>2.0.co;2.

Yano, J., M. Moncrieff, and J. McWilliams, 1998: Linear stability and single-column analyses of several cumulus parametrization categories in a shallow-water model. *Quart. Journal of the Roy. Meteor. Society*, **124**, 983-1005, doi:10.1002/qj.49712454715.